UmuD and RecA* modulate the DNA-binding activity of DNA polymerase IV in *Escherichia coli*

Authors: Sarah S. Henrikus[1,2], Amy E. McGrath[1,2], Slobodan Jergic[1,2], Matthew L. Ritger[3], Phuong T. Pham[4], Elizabeth A. Wood[3], Myron F. Goodman[5], Michael M. Cox[3], Antoine M. van Oijen[1,2], Harshad Ghodke[1,2], Andrew Robinson[1,2*]

Affiliations:

[1]Molecular Horizons Institute and School of Chemistry and Molecular Bioscience, University of Wollongong, Wollongong, Australia

[2]Illawarra Health and Medical Research Institute, Wollongong, Australia

[3]Department of Biochemistry, University of Wisconsin-Madison, USA

[4]Department of Biological Sciences, University of Southern California, Los Angeles, California, United States of America

[5]Departments of Biological Sciences and Chemistry, University of Southern California, Los Angeles, California, United States of America

Short title: Regulators of pol IV activity in *E. coli*

*Corresponding author. Mailing address: School of Chemistry and Molecular Bioscience, University of Wollongong, Wollongong, NSW 2522, Australia. Email: andrewr@uow.edu.au. Telephone: +612 4221 4735. Fax: +612 4221 4287

Abstract

Expression of DNA polymerase IV (pol IV) is increased in *Escherichia coli* cells suffering high levels of DNA damage. Despite the resulting increase in intracellular pol IV concentration, the binding of pol IV to the nucleoid does not significantly increase, indicating that pol IV activity is highly regulated in cells. Here, we use quantitative single-molecule imaging to investigate how UmuD and RecA, two binding partners of pol IV regulate its activity in live cells. We find that UmuD acts as a positive regulator of pol IV activity, promoting long-lived association of pol IV with the DNA. In contrast, its cleaved form which accumulates in DNA-damaged cells, UmuD′, acts as a negative regulator by inhibiting the binding of pol IV to DNA. In cells treated with the antibiotic ciprofloxacin, up to 40% of pol IV foci colocalise with RecA* nucleoprotein filaments. RecA(E38K), a hyperactive RecA mutant, recruits pol IV to the nucleoid, even in the absence of exogenous DNA damage. *In vitro,* RecA(E38K) forms RecA*-like structures competent of LexA cleavage, even on double-stranded DNA. Using surface plasmon resonance, we show that these RecA*-like filaments can recruit pol IV to double-stranded DNA, consistent with a physical interaction between RecA and pol IV. Together, the results show UmuD and RecA as modulators of DNA binding by pol IV and reveal new elements of a mutagenesis 'switch' that occurs in DNA damaged cells. Our findings strongly support the notion that repair synthesis during homologous recombination represents a major function of pol IV in cells.

Author Summary

In *Escherichia coli* cells exposed to DNA damaging agents, DNA repair proceeds through two phases. In the early phase, repair is predominantly error free. If damage persists, cells transition to a mutagenic repair phase. In this study we show that the activity of one repair

enzyme, DNA polymerase IV (pol IV), is modulated during these phases. In the error-free phase pol IV interacts with the UmuD protein, increasing its fidelity during DNA synthesis. We found that UmuD promotes long-lived association of pol IV with DNA, allowing ample time for synthesis to take place. During the mutagenic phase, cells contain the UmuD cleavage product, UmuD′. In addition to forming part of the highly mutagenic pol V enzyme, UmuD′ also interacts with pol IV. UmuD′ does not increase the fidelity of pol IV, thus DNA synthesis would frequently yield –1 frameshift mutations. UmuD′ however reduces this mutagenic potential by inhibiting the binding of pol IV to DNA, limiting its opportunities for DNA synthesis. We further showed that pol IV is recruited to DNA by activated forms of RecA and uncovered fresh evidence in support of double-strand break repair intermediates being major substrates for error-prone pol IV activity.

Introduction

DNA polymerase IV (pol IV), encoded by *dinB*, is one of three specialised DNA polymerases to be produced at increased levels in *Escherichia coli* cells suffering DNA damage [1]. *In vitro*, DNA polymerase IV carries out translesion synthesis (TLS) on a variety of different lesion-containing DNA substrates [2–9]. The most commonly proposed function for pol IV within cells is TLS at stalled replication forks, which may help to maintain chromosomal replication in cells experiencing DNA damage [10,11]. However, in the cell, pol IV spends most of its time at locations distal to replication forks [12]. There is significant evidence that pol IV participates in other pathways, including recombinational repair [13–19] and transcription-coupled TLS [20–23]. However, it remains unclear which of these activities are of most relevance within cells [9].

65 Single-molecule time-lapse imaging of fluorescently tagged pol IV in live *Escherichia*
66 *coli* cells revealed that various DNA-damaging agents (ciprofloxacin, UV light, methyl
67 methansulfonate [MMS]) up-regulate the production of pol IV and create binding sites for pol IV
68 [12]. Only 10% of the pol IV binding events (pol IV foci) occurred in the vicinity of replisomes.
69 At late time points during the SOS response (90–100 min after damage induction) pol IV
70 continued to form foci but no longer colocalised with replisomes, even at low levels. This led to
71 the hypothesis that replisome access might be controlled by protein–protein interactions that
72 change around 90–100 min after the induction of SOS. The results also suggest that pol IV
73 function is focused primarily on events that occur away from the replication fork.

74 The UmuD protein and its cleaved form UmuD′ have a potential role in regulating pol IV
75 activity in cells [24]. The auto-cleavage of UmuD to the shorter form UmuD′ is induced by the
76 cellular recombinase RecA, in particular RecA nucleoprotein filaments (denoted RecA*). UmuD
77 cleavage [25–27] has long been understood to be a key step in the activation of the highly
78 mutagenic enzyme DNA polymerase V (pol V) Mut ($UmuD'_2C$-RecA-ATP; [28]). Several lines
79 of evidence suggest that the conversion of UmuD to UmuD′ might also regulate the activity of
80 pol IV in *E. coli* [20]. Far-Western blots and co-purification experiments indicate that pol IV
81 interacts with $UmuD_2$ and $UmuD'_2$, but not the heterodimer UmuDD′ [20]. Overexpression of
82 pol IV induces high rates of –1 frameshift mutations in cells, which can be supressed by co-
83 overexpression of UmuD, but not co-overexpression of UmuD′ [20]. Furthermore, UmuD and
84 UmuD′ overexpression reduced frequencies in an adaptive mutagenesis assay compared to an
85 empty vector; overproduction of UmuD even lowered frequencies to equivalent levels of a
86 catalytically dead *dinB* mutant [20]. These observations have led to the proposal that UmuD
87 status regulates the mutagenic activity of pol IV-dependent DNA synthesis. Despite these

88 advances, it remains unclear if UmuD or UmuD′ affect the fidelity of pol IV or if UmuD and
89 UmuD′ also regulate the binding activity of pol IV, and thus, presumably its processivity.

90 Beyond this, a series of results indicate that pol IV operates in the repair of double-strand
91 breaks (DSBs) in live cells [15,19,29–33]. Reducing DSB formation (scavenging reactive
92 oxygen species) or introducing defects in the end-resection of double-strand breaks (Δ*recB*
93 mutation) greatly reduced the number of pol IV foci that were formed in cells treated with
94 ciprofloxacin or trimethoprim [34]. At end-resected DSBs, RecA nucleoprotein filaments
95 facilitate repair through homologous recombination [35], suggesting that pol IV should
96 colocalise with RecA* structures. A series of observations made by others support this notion.
97 Pol IV forms a physical interaction with the recombinase RecA *in vitro* and this interaction
98 modulates the fidelity of pol IV-dependent DNA synthesis [5,24,36]. This interaction is proposed
99 to provide pol IV with the ability to participate in DNA synthesis during RecA-dependent strand
100 exchange reactions [37]. In a fluorescence microscopy study [33], pol IV was shown to
101 colocalise with RecA structures *in vivo*. However, the RecA-GFP probe that was used to observe
102 RecA localisation does not differentiate between active forms of RecA (i.e. RecA*) and inactive
103 forms, such as storage structures [38]. Furthermore, this RecA-GFP (*recA4155-gfp*) probe is
104 deficient in recombination, SOS induction and UV survival [39]. It therefore remains unclear
105 whether RecA* structures, such as those that form as intermediates of recombination, represent
106 major or minor substrates for pol IV in cells. With the recent development of a RecA*-specific
107 probe, PAmCherry-mCI [38], we are now in a position to measure pol IV–RecA* colocalisation
108 directly in a time-resolved manner, probing if pol IV predominantly forms foci at homologous
109 recombination hubs.

110 In this work, we set out to test the following: 1. whether the UmuD cleavage status
111 affects the extent of pol IV focus formation at replisomes and/or the lifetimes of pol IV
112 molecules binding to DNA substrates, and 2. whether pol IV predominantly binds at RecA*
113 structures. Using single-molecule live-cell imaging, here we demonstrated that the DNA binding
114 activity of pol IV is promoted by UmuD in cells treated with the DNA damaging antibiotic
115 ciprofloxacin. In contrast, UmuD′ diminishes pol IV binding. We observed that a large
116 proportion of pol IV foci (up to 40%) colocalise with a RecA* marker. The *recA*(E38K)
117 mutation (also known as *recA730*), which constitutively produces RecA*-like activity [40–42],
118 promotes the binding activity of pol IV, even in the absence of DNA damage. We further showed
119 that this activity is due to pol IV interacting with RecA(E38K), which forms RecA*-like
120 structures on single-stranded as well as double-stranded DNA. These findings provide evidence
121 for regulatory roles for both UmuD and RecA in modulating the binding activity of pol IV in *E.*
122 *coli* cells. RecA* structures serve as major binding sites for pol IV, demonstrating a major role
123 for pol IV in homologous recombination.

124 **Results**

125 **Cleavage of UmuD affects the binding behaviour of pol IV**

126 Previously, we showed that the limited colocalisation of pol IV foci with replisome
127 markers after treatment with DNA damaging agents drops from ~10% to < 5% (i.e. baseline
128 levels; [12]) at the 90–100 min time-point. Since $UmuD_2$ and $UmuD'_2$ physically interact with
129 pol IV and modulate its mutagenic activity [24], we hypothesised that the drop in pol IV–
130 replisome colocalisation that occurs 90–100 min after the onset of DNA damage might be
131 triggered by the cleavage of UmuD to UmuD′.

132 To investigate the effect of UmuD status on pol IV activity, we compared colocalisation
133 between DinB-YPet and a DnaX-mKate2 replisome marker (coding for a fluorescent fusion of
134 the τ clamp loader protein, serving as a marker for the replisome, τ-mKate2) in four strains (all of
135 which include the *dinB-YPet dnaX-mKate2* constructs): i) *umuDC*$^{+}$ (EAW643, [12]), ii)
136 Δ*umuDC* (SSH007), iii) SSH007 expressing the non-cleavable UmuD(K97A) protein from a
137 low-copy plasmid (*dinB-YPet dnaX-mKate2* Δ*umuDC* + pUmuD[K97A], SSH007 + pJM1243),
138 and iv) SSH007 expressing the 'cleaved' UmuD′ protein from a low-copy plasmid (*dinB-YPet*
139 *dnaX-mKate2* Δ*umuDC* + pUmuD′, SSH007 + pRW66). The amount of UmuD(K97A) and
140 UmuD′ produced from each plasmid is 4–5-fold higher than UmuD expressed from its native
141 chromosomal locus [38,43].

142 Time-lapse movies were recorded for each strain after treatment with ciprofloxacin
143 (30 ng mL^{-1}). At t = 0 min, images of the DinB-YPet signal (300 ms exposure) and τ-mKate2
144 signal (replisome marker) were recorded for untreated cells. Directly after t = 0, ciprofloxacin
145 was introduced to the flow cell and a time-lapse was recorded over a period of 3 h. The numbers
146 of DinB-YPet foci per cell, reflective of pol IV binding events, were determined at 0, 30, 60, 90
147 and 120 min time points (**Fig 1**). Colocalisation between DinB-YPet foci and replisome was also
148 monitored. A complementary set of colocalisation measurements was performed, in which a
149 shorter exposure time of 50 ms was used when collecting the DinB-YPet images in order to
150 better capture transient foci (**S1 Fig**).

151 We first monitored pol IV behaviour in cells expressing wildtype levels of UmuD and
152 UmuC (EAW643, **Table 1**). Cells exhibited no pol IV foci prior to ciprofloxacin treatment (**Fig**
153 **1A**, upper panel), as seen previously [12]. After ciprofloxacin addition, the number of pol IV foci
154 per cell increased to an average of 0.1 foci per cell from 60 min, i.e. one in ten cells exhibited a

155 pol IV focus. Consistent with our previous observations [12], the percentage of pol IV foci that
156 colocalised with the replisome dropped markedly between the 90 min and 120 min time-points
157 (**Fig 1A**, middle panel). From 0–90 min after ciprofloxacin addition, 5% of pol IV foci
158 colocalised with replisomes, somewhat less than observed previously. From 120–150 min this
159 decreased to < 2%. The percentage of replisome foci that contained a pol IV focus followed a
160 similar trend (**Fig 1A**, lower panel); from 0–90 min after ciprofloxacin addition, 0.5% of
161 replisome foci contained a pol IV focus, dropping to ~0.1% (indistinguishable from chance
162 colocalisation) from 120–150 min.

163 We next examined the effect of deleting the *umuDC* operon (and thus eliminating UmuD)
164 on the number of pol IV foci and the extent of colocalisation with replisomes (SSH007, **Table**
165 **1**). From 30 min, 10–15% of pol IV foci colocalised with replisomes. Compared to *umuDC*$^+$
166 cells, Δ*umuDC* cells exhibited a 3-fold increase in the number pol IV foci per cell with ~0.3 foci
167 per cell from 60 min after ciprofloxacin addition (**Fig 1B**, upper panel). Moreover, deletion of
168 *umuDC* led to a 3-fold increase in the percentage of pol IV foci that colocalise with replisomes
169 (**Fig 1B**, middle panel). Interestingly, pol IV-replisome colocalisation now persisted above 10%
170 for the 90, 120 and 150 min time points. The percentage of replisomes that contained a pol IV
171 focus was also elevated in the Δ*umuDC* background (**Fig 1B**, lower panel). From 30 min, 2–4%
172 of replisomes contained a pol IV focus. Compared to *umuDC*$^+$ cells, this represents a 6–8-fold
173 increase in colocalisation. These observations suggest that the presence of UmuD (and/or
174 UmuD′) normally suppresses the formation of pol IV foci and also prevents pol IV from binding
175 within, or close to, replisomes.

176 We next explored the effects of expressing the non-cleavable UmuD(K97A) mutant in
177 *dinB-YPet dnaX-mKate2* Δ*umuDC* cells (SSH007 + pJM1243, **Table 1**). We note that the

178 observed effects might be slightly exaggerated because the expression level of UmuD(K97A)
179 from the plasmid is 4–5-fold higher than chromosomal levels [38,43]. At the 90 min time point,
180 cells contained on average 0.6 pol IV foci — a 6-fold increase over *umuDC*$^{+}$ cells (**Fig 1C**,
181 upper panel). This sixfold increase in pol IV foci per cell, was accompanied by a 3-fold increase
182 in colocalisation with replisomes (**Fig 1C**, middle panel). From 30 min after damage induction,
183 13% of pol IV foci formed in the vicinity of replisomes. This colocalisation remained relatively
184 constant during the later stages of the SOS response; colocalisation did not drop below 9% from
185 90–120 min as observed in *umuDC*$^{+}$ cells. These observations reveal that UmuD(K97A), and by
186 inference uncleaved UmuD, promote the binding of pol IV to DNA and do not exclude pol IV
187 from replisomes.

188 During the later stages of the SOS response (90 min after SOS induction), UmuD is
189 converted to UmuD′ [44]. To explore the effects of UmuD′ on pol IV activity, we imaged
190 Δ*umuDC* cells expressing UmuD′ directly from a plasmid (SSH007 + pRW66, **Table 1**) at 4-5
191 times higher expression levels than chromosomal expressed UmuD. These cells produced ~0.1
192 DinB-YPet foci per cell at 60 min (**Fig 1D**, upper panel), similar to *umuDC*$^{+}$ cells. In the cells
193 expressing UmuD′, colocalisation of pol IV with replisomes was generally low, but highly
194 variable (**Fig 1D**, middle panel). Two large spikes in colocalisation were apparent at the 30 and
195 90 min time points. However, due to the low number of foci available for analysis at these time-
196 points, there was very large error associated with these values. No spikes in colocalisation were
197 observed when measuring the proportion of replisomes that contained a pol IV focus (**Fig 1D**,
198 lower panel). Importantly, the colocalisation of pol IV with replisomes decreased to < 1% after
199 90 min (**Fig 1D**, middle panel). Similarly, the percentage of replisomes with that contained a pol
200 IV focus drops between the 90 and 120 min time points (**Fig 1D**, lower panel). From 30–90 min,

201 ~1% of replisomes contained a pol IV focus. By 120 min < 0.1% of replisomes contained a pol
202 IV focus. Overall, the introduction of UmuD′ into Δ*umuDC* cells restores rates of focus
203 formation and colocalisation with replisomes to near wild-type (*umuDC*$^{+}$) levels.

204 Taken together, the time-lapse imaging results show that the presence of non-cleavable
205 UmuD results in an increase in pol IV binding events in cells, accompanied by greater access to
206 the replisomes during the late SOS response (90-120 min). Similarly, cells lacking UmuDC
207 exhibit a greater number of pol IV binding events during the late SOS response (90-120 minute
208 window), accompanied by greater access of pol IV to replisomes at these time points.
209 Importantly, the maximum extent of colocalisation of pol IV with replisomes in both cases was
210 similar, with a maximum at ~ 15%. This suggests that even though greater replisome access is
211 permitted in cells lacking UmuDC or carrying the non-cleavable UmuD, replisomes do not
212 represent the major binding substrate for pol IV, during the SOS response. Strikingly, UmuD′
213 suppresses binding of pol IV to the nucleoid, including at replisomal sites. These results suggest
214 that UmuD cleavage is a biochemical switch for pol IV activity.

215 **UmuD(K97A) but not UmuD′ provides long-lived replisome access to pol IV**

216 Time-lapse imaging revealed differences in pol IV activity in *umuDC* variants with
217 respect to the number of foci per cell and access to replisomes. We noted that in the various
218 DinB-YPet images the foci formed in different strains appeared to exhibit differences in both
219 intensity and shape (**Fig 2A–D**, first row; 300 ms exposures). For the *umuDC*$^{+}$ (**Fig 2A**),
220 Δ*umuDC* (**Fig 2B**) and UmuD′-expressing cells (**Fig 2D**), most foci were relatively faint and
221 diffuse. In contrast, cells expressing UmuD(K97A) produced brighter, and much more distinct,
222 pol IV foci. Reasoning that these differences might reflect differences in the nature of pol IV
223 interactions with the substrates, we next measured the binding lifetime of pol IV at these sites.

224 Image sets were recorded during three periods following the addition of ciprofloxacin: 20–45
225 min, 55–85 min and 120–180 min. For each time interval and each strain (EAW643, SSH007,
226 SSH007 + pJM1243, SSH007 + pRW66; **Table 1**), burst acquisitions of the DinB-YPet signal
227 were recorded (300 images of 34 ms exposure time, total length of 10.2 s). Subsequently, a
228 corresponding image of the replisome marker τ-mKate2 was collected (see **S2B Fig** for imaging
229 sequence).

230 For the *umuDC*$^{+}$, Δ*umuDC* and UmuD′-expressing cells, intensity trajectories collected at
231 replisomal positions predominantly exhibited short-lived binding events (**Fig 2**, second row).
232 Cells expressing UmuD(K97A), on the other hand, often produced long-lived pol IV binding
233 events. To comprehensively assess the binding lifetimes of pol IV with respect to the UmuD
234 status at sites of replisomes, mean autocorrelation functions were calculated for foci within each
235 strain (**Fig 2**, third row; **S2 Fig**). This approach allows us to extract characteristic timescales of
236 signal fluctuations within intensity trajectories, which reflect the lifetimes of binding and
237 dissociation events. Exponential fitting of each mean autocorrelation function gave time
238 constants of $\tau = < 0.03$, 0.3 and 3.3 s, reflecting short-, medium-, and long-lived binding events
239 (**S2 Fig**). For each strain and time interval after ciprofloxacin addition, the relative proportions of
240 these binding events are plotted in **Fig 2** (fourth row).

241 For both *umuDC*$^{+}$ and Δ*umuDC* cells, most pol IV binding at replisomes is short-lived
242 (**Fig 2A, B**). In the early stages of ciprofloxacin exposure (25–45 min) the components of the
243 autocorrelation function were 80% short-lived, 10% medium and 10% long-lived. In the later
244 stages, (120–150 min), the proportion of medium-long lived events increased to 40%. In cells
245 expressing UmuD(K97A) long-lived events were much more common: by the 120–150 min
246 period medium and long-lived events comprised 80% of the autocorrelation function (**Fig 2C**). In

247 stark contrast, cells expressing UmuD′ produced almost exclusively short-lived events (**Fig 2D**).
248 UmuD′ appeared to supress the medium and long-lived pol IV binding events that occur in wild-
249 type *umuDC*$^{+}$ background following ciprofloxacin treatment.

250 Taken together, the results indicate that UmuD(K97A) promotes long-lived DNA binding
251 by pol IV, whereas UmuD′ inhibits binding. The deletion of *umuDC* only marginally increases
252 the binding lifetime of pol IV compared to *umuDC*$^{+}$. The results demonstrate that pol IV binding
253 activity is modulated by UmuD and UmuD′ in cells.

254 **Pol IV binds frequently at RecA* structures**

255 Like UmuD and UmuD′, the RecA recombinase modulates the mutagenic activity of pol
256 IV [14,17]. *In vitro*, DNA synthesis by pol IV is error-prone when operating on D-loop
257 substrates that mimic recombination intermediates [14,17]. Pol IV is known to participate in
258 error-prone DSB repair under a variety of circumstances [13–19,30,32]. It however remains to be
259 determined whether sites of DSB repair represent minor or major substrates for pol IV *in vivo*.

260 We determined whether pol IV colocalises with RecA* structures by visualising the
261 localisations of fluorescent pol IV (DinB-YPet) and a RecA* marker (PAmCherry-mCI; a red
262 fluorescent protein fusion of a monomeric C-terminal fragment of the λ repressor that retains the
263 ability to bind RecA* in cells [38]) in SSH092 cells treated with ciprofloxacin — a potent
264 inducer of DSBs [45,46] which also causes the accumulation of reactive oxygen species
265 potentiating killing [47]. Live cell photoactivatable localisation microscopy (PALM) of SSH092
266 cells treated with ciprofloxacin was performed by collecting images in both channels every 5 min
267 over a period of 3 h following introduction of ciprofloxacin at time point t = 0 min. At each time
268 point, a new field-of-view was recorded.

269 Following ciprofloxacin treatment, cells typically contained multiple RecA* structures
270 (**Fig 3A**), including both foci at early time points, and more elongated "bundle" structures
271 described previously at later time points [38]. We next determined the percentage of DinB-YPet
272 foci that colocalised with RecA* features (**Fig 3B**). Prior to the introduction of ciprofloxacin,
273 RecA* filaments were rarely formed in cells during normal metabolism (< 0.1 mCI foci per cell)
274 consistent with our previous study [38]. Unsurprisingly, we did not detect colocalisation of pol
275 IV with RecA* in untreated cells. Upon introduction of ciprofloxacin to the flow chamber,
276 colocalisation remained low during the early phase of the SOS response (i.e., between 0–45 min
277 after treatment). From 45 min after the introduction of ciprofloxacin, pol IV exhibited extensive
278 colocalisation (10–40%) with RecA* structures in cells. This extensive colocalisation persisted
279 into the late stages of SOS (up to 180 min after treatment). We have previously noted that most
280 of the RecA* foci form at locations distal to the replisome [38].

281 **RecA* promotes the binding of pol IV to the nucleoid**

282 Having observed that a large proportion of pol IV colocalises with RecA*, we next set
283 out to determine whether RecA* recruits pol IV to the DNA, characterising the ability of pol IV
284 to bind RecA* structures. Therefore, we utilised a RecA mutant, RecA(E38K), which is able to
285 constitutively induce SOS in cells [40–42,48], suggestive of the formation of RecA* structures
286 being formed in the absence of endogenous DNA damage.

287 Using surface plasmon resonance (SPR), we here showed that RecA(E38K) forms
288 filaments on ssDNA *in vitro* (**S3A, B Fig**). Stable association of RecA(E38K) required the
289 presence of ATPγS suggesting that RecA(E38K) forms filaments (**S3B Fig**). Additionally,
290 RecA(E38K) filaments on ssDNA are competent to cleave LexA (**S4 Fig**), suggesting that
291 RecA(E38K) forms RecA*-like structures on ssDNA [27,49]. However, in the absence of DNA

292 damage, we expect exposed ssDNA substrates for RecA(E38K) binding to occur infrequently.
293 Therefore, we additionally tested whether constitutive SOS signalling may occur due to
294 constitutive RecA(E38K)-dsDNA filament formation. To that end, we tested the ability of
295 RecA(E38K) to form filaments on a 60-mer dsDNA substrate. We found that RecA(E38K) binds
296 to dsDNA (**S3C, D Fig**) and that incubation of dsDNA plasmid substrates with RecA(E38K)
297 promoted LexA cleavage (**S4 Fig**), indicating that RecA(E38K) forms RecA*-like structures on
298 dsDNA [27,49].

299 Together, these results allowed us to establish conditions where we could now probe the
300 binding of pol IV to constitutive RecA filaments even in the absence of DNA damage in live
301 cells. We performed single-molecule imaging of *dinB-YPet dnaX-mKate2* cells carrying wild-
302 type or mutant alleles of *lexA* (encoding the SOS-response repressor LexA) and *recA* (encoding
303 the recombinase RecA). Three strains were examined: i) cells with wild-type *lexA* and *recA*
304 alleles (EAW643, *dinB-YPet dnaX-mKate2 lexA*$^+$ *recA*$^+$, **Table 1**), ii) cells that constitutively
305 express high levels of DinB-YPet even in the absence of exogenous DNA damage (and all other
306 SOS-induced proteins [49]; RW1594, *dinB-YPet dnaX-mKate2 lexA*[Def] *recA*$^+$, **Table 1**) and
307 iii) cells that both produce high levels of DinB-YPet and constitutively formed RecA*-like
308 structures (RW1598, *dinB-YPet dnaX-mKate2 lexA*[Def] *recA*[E38K], **Table 1**) [40–42,48].

309 We set out to determine if the presence of RecA*-like structures formed by RecA(E38K)
310 is sufficient to recruit pol IV to the nucleoid in cells. We recorded burst acquisitions of DinB-
311 YPet motions in the three strains (300 images of 34 ms exposure time, total length of 10.2 s). For
312 each movie, a corresponding image of the replisome marker τ-mKate2 was also captured (see
313 **S2A, B Fig** for imaging sequence). As expected, with wild-type *lexA* and *recA* alleles cells
314 produced few pol IV foci (**Fig 4A**) [12]. Cells that carried the SOS-constitutive *lexA*(Def) allele

315 and the wild-type *recA* allele produced a relatively high level of DinB-YPet signal, but produced
316 few foci (**Fig 4B**) [12]. This result is consistent with our previous study in which we concluded
317 that binding is triggered by the presence of damage on the DNA, as opposed to mass action-
318 driven exchange brought on by increased intracellular concentrations of pol IV [12]. In contrast
319 to both *recA*$^+$ strains, cells carrying both the *lexA*(Def) allele and the RecA*-constitutive
320 *recA*(E38K) allele produced both high DinB-YPet signal and readily visible foci (**Fig 4C**). These
321 results suggest two possibilities: first, that in the absence of ciprofloxacin induced double strand
322 breaks, *lexA*(Def) *recA*(E38K) cells exhibit DNA substrates for pol IV that are not present in
323 *lexA*(Def) cells carrying wild-type RecA; and second, that nucleoid associated RecA(E38K)
324 assemblies are themselves substrates for pol IV in these cells.

325 We therefore directly tested whether RecA(E38K) interacts with pol IV on filaments
326 assembled dsDNA *in vitro*. Using an identical SPR experimental setup [38], we assembled
327 RecA(E38K) on a 60-mer dsDNA substrate (**S3C, D Fig**). We found that pol IV associates with
328 RecA(E38K)-ATPγS filaments formed on dsDNA (**S3E Fig**) comparing to pol IV association
329 with dsDNA (**S3F Fig**) Unfortunately, non-specific binding of pol IV to the chip surface,
330 hampered our attempts to extract binding parameters from the sensorgrams. Nevertheless, these
331 results clearly demonstrate that the association of pol IV with the nucleoid is promoted by the
332 presence of RecA*-like structures.

333 Using the single-molecule data, we next examined fluctuations in the DinB-YPet signals
334 that occur as pol IV binds to, or dissociates from, its binding site. Both replisomal and non-
335 replisomal positions within cells were monitored. Intensity trajectories for DinB-YPet in *lexA*$^+$
336 *recA*$^+$ cells and *lexA*(Def) *recA*$^+$ cells predominantly showed short-lived spikes (< 1s; **Fig 4D, E**),
337 indicative of transient pol IV binding events (milliseconds timescale). In contrast, trajectories for

338 DinB-YPet in *lexA*(Def) *recA*(E38K) cells often included binding events that were much longer
339 lived (1–10s, **Fig 4F**), indicative of pol IV binding to its target for longer periods (seconds
340 timescale).

341 To comprehensively assess pol IV binding lifetimes across all intensity trajectories, mean
342 autocorrelation functions were calculated for each set of trajectories (**S2D–F Fig**). Fitting of each
343 autocorrelation function give time constants $\tau = < 0.03$, 0.4 and 6.0 s, reflecting short-, medium-,
344 and long-lived binding events (**Fig 4G, H**; **S2G, H Fig**). For *lexA*$^+$ *recA*$^+$ cells in the absence of
345 ciprofloxacin, only 1% of replisomes showed evidence of pol IV binding events (**Fig 4G**, right
346 panel). The normalised mean autocorrelation function for *lexA*$^+$ *recA*$^+$ cells was of low amplitude
347 (0.16 at Δt = 1 frame, **Fig 4G**, black line), indicative of there being relatively few long-lived
348 binding events at replisomes across the different trajectories [12]. The *lexA*(Def) *recA*$^+$
349 background marginally increased pol IV binding activity with 5% of replisomes being visited by
350 DinB-YPet (**Fig 4G**, right panel) [12]. The autocorrelation function remained of low amplitude
351 (0.3 at Δt = 1 frame, **Fig 4G**, black line), indicating that few long-lived pol IV binding events
352 occurred at replisomes in the *lexA*(Def) *recA*$^+$ background. In contrast, *lexA*(Def) *recA*(E38K)
353 cells exhibited a strong increase in pol IV binding activity, both close to and away from
354 replisomes; 31% of replisomes experienced a pol IV binding event (**Fig 4G**, right panel). The
355 amplitude of the autocorrelation function was also increased (0.4 at Δt = 1 frame, **Fig 4G**, black
356 line), indicating that long-lived binding events occurred at replisomes much more frequently.
357 The decay rate of the autocorrelation function had two components (**Fig 4G**, right panel: $\tau_m = 0.4$
358 s with an amplitude of 15% and $\tau_l = 6.0$ s with an amplitude of 29%), suggesting that pol IV
359 typically binds in the vicinity of replisomes for periods of a few seconds in the *recA*(E38K)

360 background. When analysing the binding behaviour of pol IV away from replisomes in these
361 three backgrounds, similar results were obtained (**Fig 4H**).

362 **Discussion**

363 In this study, we arrived at four conclusions: i) UmuD promotes the binding of pol IV to
364 DNA, at both replisomal and non-replisomal sites; ii) UmuD′ inhibits the binding of pol IV to
365 DNA, at both replisomal and non-replisomal sites; iii) pol IV frequently colocalises with RecA*
366 structures; iv) RecA*-like structures promote the binding of pol IV to the DNA. These results
367 lead us to infer that RecA*-like structures can recruit pol IV to the nucleoid. Following
368 ciprofloxacin treatment, this pol IV-RecA* interaction might facilitate pol IV operating at DSB
369 repair intermediates. Further, the RecA* mediated cleavage of UmuD, a biochemical switch that
370 has long been known to regulate pol V activation, also regulates DNA binding by pol IV. The
371 results strongly support roles for both RecA and UmuD as regulatory factors for pol IV *in vivo*,
372 as proposed previously [5,14,17,24,36].

373 **$UmuD_2$ and $UmuD'_2$ as regulators of pol IV**

374 A previous study suggested that both $UmuD_2$ and $UmuD'_2$ bind to pol IV and modulate
375 its mutagenic activity [24]. Moreover, *in vitro* experiments have suggested that full-length
376 UmuD binds to the replicative polymerase, α, and destabilises its interaction with the sliding
377 clamp, β, thus facilitating other polymerases, such as pol IV, to access the replisome [50,51].

378 Here we show that UmuD increases the number of pol IV foci and the binding time of pol
379 IV at the nucleoid. In contrast, UmuD′ inhibits the DNA-binding activity of pol IV. During the
380 first stage of the SOS response, most UmuD is present as full-length $UmuD_2$. This would
381 promote long-lived binding of pol IV to DNA in a high-fidelity state. Based on rates of pol IV-

382 dependent DNA synthesis measured *in vitro* (3–5 nt s^{-1}; [52]), binding events lasting a few
383 seconds, such as those observed during this study, could permit the incorporation of tens of
384 nucleotides. Based on the high degree of colocalisation we observe between pol IV and RecA*,
385 as well as the strong *recB*-dependence for pol IV focus formation [34], we presume that most of
386 these early events would occur at DSB repair intermediates.

387 This work allows us to propose the following model for pol IV activity in the context of
388 the SOS response. Cells experiencing extensive DNA damage trigger the full extent of the SOS
389 response, leading to the formation of UmuD′ at late time points after DNA damage. At this point,
390 the cell enters a mutagenic phase. The highly error-prone polymerase pol V Mut becomes active
391 and pol IV, now in the absence of UmuD, introduces –1 frameshift mutations. At the same time
392 pol IV binding becomes infrequent and short-lived in the presence of UmuD′, consistent with an
393 earlier observation that UmuD′ reduces the frequency of adaptive mutagenesis [24]. Thus, while
394 pol IV is error-prone in the presence of UmuD′, mutagenesis would be kept in check by pol IV
395 having reduced access to substrates. This mechanism is in line with the multiple mechanisms that
396 have evolved to restrict the mutagenic activity of pol V [53].

397 **Pol IV as a recombination protein**

398 The high degree of colocalisation we observed between pol IV and RecA*, together with
399 the RecA*-like structures promoting pol IV binding events, adds to a growing body of evidence
400 supporting the participation of pol IV in homologous recombination [13–19,29,30,32]. Pol IV
401 colocalises with RecA* (this study) far more frequently than it colocalises with replisomes [12].
402 In addition, defects in DSB processing strongly suppress both pol IV up-regulation and focus
403 formation [34]. Interestingly, *in vitro*, pol IV is capable of associating with RecA(E38K)-ATPγS
404 filaments formed on dsDNA. These filaments are competent of LexA cleavage, indicative of

405 RecA*-like structures. *In vivo* in the absence of DNA damage, pol IV forms foci in the
406 *recA*(E38K) mutant, suggestive of pol IV binding to RecA(E38K) filaments, which presumably
407 form on dsDNA. An interaction between pol IV and RecA likely facilitates the recruitment of pol
408 IV to homologous recombination intermediates.

409 The results presented here indicate that in ciprofloxacin-treated cells the primary pathway
410 in which pol IV functions in cells is homologous recombination, as opposed to translesion
411 synthesis at replisomes as is most commonly proposed [11,54,55]. The most likely role for pol
412 IV in this process is the extension of D-loops during repair synthesis [14,17,36]. The association
413 of pol IV with RecA is however general [24] and error-prone DNA synthesis by pol IV may not
414 require RecA* filaments on processed ssDNA intermediates.

415

416 **Materials and Methods**

417 *Strain construction, plasmid construction and transformations*

418 SSH007 is a two-colour strain (*dinB-YPet dnaX-mKate2* Δ*umuDC*) derived from
419 EAW643 (*dinB-YPet dnaX-mKate2*). It was made by replacing the wild-type *umuDC*$^{+}$ gene of
420 EAW643 Δ*umuDC*::Cm^{R} from RW880 via P1 transduction. Colonies were selected by testing
421 for chloramphenicol resistance.

422 To investigate the influence of UmuD mutants on pol IV activity, SSH007 was
423 complemented with plasmids that express UmuD(K97A) (pJM1243) or UmuD′ (pRW66).

424 SSH092 was made by transformation; EAW633 (*dinB-YPet*) carries the pJMuvrA-
425 PAmCherry-mCI vector (see **Supplementary Notes** for sequence). The PAmCherry-mCI gene
426 block was commercially synthesised and the sequence was verified (IDT gene block). The gene
427 block was introduced into pSC101 [43] using the *Apa*I and *Sac*II restriction sites.

428 RW1598 was made by P1 transduction of *recA730 srlD300*::Tn*10* from RW244 into
429 RW1594, selecting for TetR. Colonies were then screened for constitutive UmuD cleavage using
430 Western blotting. *recA* and *srlD* are about 90% linked.

431 pJM1243 was made by chemically synthesizing an *E.coli* codon optimised *umuD*(K97A)
432 gene that was cloned into the low-copy spectinomycin resistant vector, pSC101 [43], as *Hin*dIII-
433 *Eco*RI fragment. UmuD(K97A) expression is LexA-regulated. Similarly, pRW66 was made by
434 introducing the *umuD′* gene into pSC101 [43].

435 **Table 1.** Strains used in this study.

Strain	Relevant Genotype	Parent strain	Source/technique
MG1655	*dinB*$^{+}$ *umuDC*$^{+}$ *lexA*$^{+}$*recA*$^{+}$	-	[56]

RW1594	*dinB-YPet dnaX-mKate2 sulA::kan*^{R} *lexA*(Def) Cm^R	RW1588	[12]
RW244	*recA*(E38K) *srlD300*::Tn10	-	[57]
RW1598	*dinB-YPet dnaX-mKate2 sulA*::kan^R *lexA*(Def)::Cm^R *recA*(E38K) *srlD300*::Tn*10*	RW1594	Transduction of RW1594 with P1 grown on RW244
EAW633	*dinB-YPet*::kan^R	MG1655	[12]
EAW643	*dinB-YPet*::FRT *dnaX-mKate2*::kan^R *lexA*$^+$	EAW633	[12]
RW880	Δ*umuDC*::Cm^R	MG1655	[34]
SSH007	*dinB-YPet*::FRT *dnaX-mKate2*::kan^R *lexA*$^+$ Δ*umuDC*::Cm^R	EAW643	Transduction of EAW643 with P1 grown on RW880
SSH007 + pJM1243	*dinB-YPet*::FRT *dnaX-mKate2*::kan^R *lexA*$^+$ Δ*umuDC*::Cm^R (chr) + UmuD(K97A) (pl)	SSH007	Transformation of SSH007 with pJM1243
SSH007+ pRW66	*dinB-YPet*::FRT *dnaX-mKate2*::kan^R *lexA*$^+$ Δ*umuDC*::Cm^R (chr) + UmuD′ (pl)	SSH007	Transformation of SSH007 with pRW66
SSH092	*dinB-YPet*::kan^R (chr) + PAmCherry-mCI (pl)	EAW633	Transformation of EAW633 with pJMuvrA-PAmCherry-mCI [38]

436

437 *Fluorescence microscopy and imaging protocols*

438 For all experiments except for experiments including imaging of PAmCherry-mCI, wide-
439 field fluorescence imaging was performed on an inverted microscope (IX-81, Olympus with a

440 1.49 NA 100× objective) in an epifluorescence configuration, as described previously [58].
441 Continuous excitation is provided using semidiode lasers (Sapphire LP, Coherent) of the
442 wavelength 514 nm (150 mW max. output) and 568 nm (200 mW max. output). τ-mKate2 was
443 imaged using yellow excitation light (λ = 568 nm) at high intensity (2750 W cm^{-2}), collecting
444 emitted light between 610–680 nm (ET 645/75m filter, Chroma) on a 512 × 512 $pixel^2$ EM-CCD
445 camera (C9100-13, Hamamatsu). For DinB-YPet time-lapse imaging, we used green excitation
446 (λ = 514 nm) at lower power (240 W cm^{-2}), collecting light emitted between 525–555 nm
447 (ET540/30m filter, Chroma).

448 For experiments including imaging of PAmCherry-mCI, imaging was conducted on an
449 inverted microscope (Nikon Eclipse-Ti), equipped with a 1.49 NA 100× objective and a 512 ×
450 512 $pixel^2$ Photometrics Evolve CCD camera (Photometrics, Arizona, US). NIS-Elements
451 equipped with JOBS module was used to operate the microscope (Nikon, Japan). Continuous
452 excitation is provided using semidiode lasers of the wavelength 405 nm (OBIS, Coherent, 200
453 mW max. output), 514 nm (Sapphire LP, Coherent, 150 mW max. output) and 568 nm (Sapphire
454 LP, Coherent, 200 mW max. output). DinB-YPet was imaged using green excitation (λ = 514
455 nm) at lower power (~2200 W cm^{-2}), collecting light emitted between 535–550 nm (ET535/30m
456 filter, Chroma). PAmCherry-mCI was imaged by simultaneous illumination with the activation
457 laser 405 nm (1–5 W cm^{-2}) and 568 nm readout laser (540 W cm^{-2}), a PALM (photoactivation
458 localisation microscopy) acquisition protocol, collecting emitted light from 590 nm (ET590LP,
459 Chroma).

460 Burst acquisitions (movies of 300 × 34 ms frames, continuous excitation with 514 nm
461 light; each frame at 80 W cm^{-2}) were collected to characterise DinB-YPet binding kinetics;
462 followed by a set of two images (bright-field [34 ms exposure]; mKate2 fluorescence [100 ms

463 exposure]). Data were recorded from 20–45 min, from 55–85 min and from 120–180 min after
464 ciprofloxacin treatment (30 ng mL^{-1}). Time-lapse movies were recorded to visualise changes in
465 DinB-YPet binding activity and measure colocalisation with the replisome marker. Sets of three
466 images were recorded (bright-field [34 ms exposure], YPet fluorescence [50 ms exposure];
467 mKate2 fluorescence [100 ms exposure]) at an interval of 10 min for 3 h. All images were
468 analysed with ImageJ [59].

469 Time-sampling of DinB-YPet and PAmCherry-mCI expressing cells were performed as
470 follows: First, the bright-field image was taken with 100 ms exposure time. Then, a PALM
471 acquisition protocol (simultaneous illumination with the activation laser 405 [1–5 W cm^{-2}] and
472 568 nm readout laser [540 W cm^{-2}] for 200 frames taken every 100 ms) was used to image
473 PAmCherry-mCI. Third, DinB-YPet was detected using 512 nm laser (50 ms exposure time at
474 ~2200 W cm^{-2}). The experiment was performed over 3 h, time points were sampled at an interval
475 of 5 min. At each time point, a new field-of-view was sampled to minimise laser-induced
476 damage.

477 To image DinB-YPet and PAmCherry-mCI, sets of three acquisitions were recorded
478 (bright-field [100 ms exposure], YPet fluorescence [50 ms exposure]; PAmCherry fluorescence
479 [simultaneous illumination with the activation laser 405 and 568 nm readout laser for 200 frames
480 each with 100 ms exposure]). This protocol was only executed once for a field-of-view to
481 minimise laser damage. Consequently, each time point shows a new set of cells. The experiment
482 was conducted over 3 h, an image was taken every 5 min.

483 *Flow cell design*

484 All imaging was carried out on cultures growing in home-built flow cells. Imaging was
485 carried out in quartz-based flow cells, similar to those used in our previous study [12]. These

486 flow cells were assembled from a no. 1.5 coverslip (Marienfeld, reference number 0102222 or
487 0107222), a quartz top piece (45 × 20 × 1 mm^3) and PE-60 tubing (Instech Laboratories, Inc.).
488 Prior to flow cell assembly, coverslips were silanized with aminopropyltriethoxy silane (APTES;
489 Alfa Aeser). First, coverslips were sonicated for 30 min in a 5M KOH solution to clean and
490 activate the surface. The cleaned coverslips were rinsed thoroughly with MilliQ water, then
491 treated with a 5% (v/v) solution of APTES in MilliQ water. The coverslips were subsequently
492 rinsed with ethanol and sonicated in ethanol for 20 s. Afterwards, the coverslips were rinsed with
493 MilliQ water and dried in a jet of N_2. Silanised slides were stored under vacuum prior to use.

494 To assemble each flow cell, polyethylene tubing (BTPE-60, Instech Laboratories, Inc.)
495 was glued (BONDiT B-482, Reltek LLC) into two holes that were drilled into a quartz piece.
496 After the glue solidified overnight, double-sided adhesive tape was stuck on two opposite sides
497 of the quartz piece to create a channel. Then, the quartz piece was stuck to an APTES-treated
498 coverslip. The edges were sealed with epoxy glue (5 Minute Epoxy, DEVCON home and Epoxy
499 Adhesive, 5 Minute Everyday, PARFIX). Each flow cell was stored in a desiccator under mild
500 vacuum while the glue dried. Typical channel dimensions were 45 × 5 × 0.1 mm.

501 *Setup of flow cell experiments*

502 For all imaging experiments, cells were grown at 37 °C in EZ rich defined medium
503 (Teknova) that contained 0.2% (w/v) glucose. EAW643, RW1594 and RW1598 cells were
504 grown in the presence of kanamycin (25 μg mL^{-1}), SH001 cells were grown in the presence of
505 chloramphenicol (25 μg mL^{-1}), SSH007 cells carrying pJM1243 or pRW66 were grown in the
506 presence of spectinomycin (50 μg mL^{-1}). Cells carrying PAmCherry-mCI were also grown in the
507 presence of spectinomycin (50 μg mL^{-1}). Cells were loaded into flow cells, allowed a few
508 minutes to associate with the APTES surface, then, loosely associated cells were removed by

509 pulling through fresh medium. The experiment was then initiated by switching the medium to a
510 medium that contains 30 ng mL^{-1} ciprofloxacin (for cells carrying plasmids: 50 μg mL^{-1}
511 spectinomycin was added). A flow rate of 50 μL min^{-1} was applied during the experiment to
512 allow a constant nutrient and oxygen supply by using a syringe pump.

513 *Proteins*

514 The wild-type *E. coli* RecA protein was purified as described [60]. The RecA
515 concentration was determined using the extinction coefficient $\varepsilon_{280} = 2.23 \times 10^4\ M^{-1}\ cm^{-1}$ [60].

516 The *E. coli* RecA(E38K) protein was purified as previously described [61] with the
517 following modifications. After washing the protein pellet with R buffer plus 2.1 M ammonium
518 sulfate, the pellet was resuspended in R buffer plus 1 M ammonium sulfate. The sample was
519 loaded onto a butyl-Sepharose column and washed with 1.5 column volumes of R buffer plus 1
520 M ammonium sulfate. It was then eluted with a linear gradient from R buffer plus 1 M
521 ammonium sulfate to R buffer, carried out over 5 column volumes. Peak fractions were
522 identified by SDS-PAGE analysis and pooled. The protein was loaded onto a hydroxyapatite
523 column as done previously, but with the linear gradient from 10 to 500 mM P buffer. The
524 fractions were dialyzed against R buffer plus 50 mM KCL and 1 mM DTT three times. The
525 fractions were loaded onto a Source 15S column and washed with R buffer plus 50 mM KCl and
526 1 mM DTT until the UV trace receded from peak. Next, the pool was loaded onto a Source 15Q
527 column and eluted with a linear gradient from 50 mM KCl to 1 M KCl over 25 column volumes.
528 Peak fractions were identified as above and pooled. A DEAE-Sepharose column was not used.
529 Protein in this pool was precipitated by the addition of equal volume of 90% saturated
530 ammonium sulfate. The precipitate was stirred and then spun down at 13,000 rpm for 30 min.
531 The pellet was resuspended in R buffer plus 1 M ammonium sulfate, stirred for an hour, and then

532 spun down again. This protein was loaded onto a butyl-Sepharose column and eluted in a
533 gradient from R buffer and 1 M ammonium sulfate to R buffer. The fractions were identified,
534 pooled, and concentrated using GE Vivispin 20 10K MWCO centrifuge filter concentrating
535 units. The protein was flash frozen in liquid nitrogen and stored at -80˚C. The concentration was
536 determined as above. No exonuclease or other endonuclease activities were detected.

537 Pol IV (*dinB*) coding sequence was cloned into NcoI and BamHI sites of pET16b to
538 generate a native pol IV expression construct. *E. coli* strain Turner/pLysS (Novagen) carrying
539 the expression construct was grown in LB medium supplemented with 20 μg/ml
540 chloramphenicol and 100 μg/ml ampicillin. Expression of pol IV was induced by adding IPTG to
541 1 mM and growing for 3-4 h at 30°C. Collected cells (~20 g) were resuspended in 50 mL of lysis
542 buffer (50 mM Tris-HCl, pH 7.5, 1 M NaCl, 10% sucrose, 2 mM DTT, 1 mM EDTA and
543 protease inhibitor cocktails). Cells were lysed by lysozyme (2 mg/mL) and the clarified extract
544 was collected following centrifugation at 15000 x g for 30 min. Pol IV was then precipitated by
545 ammonium sulfate added to 30% saturation and stirring for 10 min. The precipitate was
546 subjected to gel-filtration in GF-buffer (20 mM Tris-HCl, pH 7.5, 1 M NaCl, 0.1 mM EDTA, 1
547 mM DTT) using a GE Healthcare Superdex-75 XK-26/60 gel filtration column. Pol IV fractions
548 were pooled, dialyzed overnight in PC-buffer (20 mM Tris-HCl, pH 7.5, 0.1 mM EDTA 1 mM
549 DTT, 10% Glycerol), containing 200 mM NaCl and then subjected to phosphocellulose
550 chromatography (P-11, Whatman). After washing extensively with PC-buffer + 200 mM NaCl,
551 pol IV was eluted with a linear gradient of 200 mM to 500 mM NaCl. Fractions containing
552 native pol IV (>99% pure) were pooled and stored at –70°C.

553 *Surface Plasmon Resonance (SPR) experiments*

554 SPR experiments were conducted on BIAcore T200 istrument (GE Healthcare) using
555 streptavidin (SA) coated sensor chips, probing the formation of RecA structures (assembled from
556 RecA[E38K]) on ssDNA and dsDNA. Experiments were carried out at 20 °C at a flow rate of 5
557 μL min^{-1}. As described previously [38], SA chips were activated and stabilised, single-stranded
558 biotinylated 71-mer poly-dT oligonucleotide bio-$(dT)_{71}$ was immobilised, followed by
559 RecA(E38K) filament assembly (**S3A, B Fig**). RecA(E38K) filaments were assembled on bio-
560 $(dT)_{71}$ by injecting 1 μM RecA(E38K) in $SPR^{RecA(E38K)}$ buffer (20mM Tris-HCl, pH 8.0, 10 mM
561 KCl, 10 mM $MgCl_2$, 0.005% surfactant P20 and 0.5 mM dithiothreitol) supplemented with 1 mM
562 adenosine 5'-(γ-thio) triphosphate (ATPγS) at 10 μL min^{-1} for 400 s. Similarly, biotinylated
563 dsDNA was immobilised (as previously described [38]), followed by RecA(E38K) filament
564 assembly (**S3C, D Fig**). RecA(E38K) filaments were assembled on dsDNA (sequence: 5'-TCC
565 TTT CGT CTT CAA AGT TCT AGA CTC GAG GAA TTC TAA AGA TCT TTG ACA GCT
566 AGC CAG-3', 5' end is biotinylated) by injecting 1 μM RecA(E38K) in $SPR^{RecA(E38K)}$ buffer
567 (20mM Tris-HCl, pH 8.0, 10 mM KCl, 10 mM $MgCl_2$, 0.005% surfactant P20 and 0.5 mM
568 dithiothreitol) supplemented with 0.5 mM ATPγS at 5 μL min^{-1} for 500 s. Then, $SPR^{RecA(E38K)}$
569 supplemented with 0.5 or 1 mM ATPγS buffer was flowed in at 5 μL min^{-1} for 2,500 s, in order
570 to stabilise the formed filaments. From 3,000 s, 1 μM RecA(E38K) in $SPR^{RecA(E38K)}$ buffer
571 supplemented with 0.5 mM ATPγS was injected at a flow rate of 5 μL min^{-1} for 4,200 s.

572 Pol IV association with RecA(E38K)-dsDNA filaments was observed by injecting 0.65
573 μM pol IV in $SPR^{RecA(E38K)}$ buffer supplemented with 0.5 mM ATPγS for 220 s at 5 μL min^{-1},
574 monitoring pol IV association (**S3E Fig**). From 220 s, buffer containing 0.5 mM ATPγS was
575 flowed in at 5 μL min^{-1} and fast dissociation of pol IV was observed. Similarly, pol IV

576 association with dsDNA was monitored, giving a lower response curve (**S3F Fig**). We also
577 observed non-specific binding of pol IV to the chip surface, making it impossible to measure
578 binding kinetics of pol IV.

579 The surface was regenerated as previously reported [38]. Furthermore, the SPR signal
580 were corrected using a flow cell without immobilised bio-$(dT)_{71}$ or dsDNA and corrected for the
581 amount of immobilised RecA(E38K) [38]. Ghodke *et al.* utilised this assay to monitor the
582 binding kinetics of mCI at RecA-ssDNA filament [38].

583 *DNA Substrates for ATPase and LexA Cleavage Assay*

584 M13mp18 cssDNA was purified as previously described [62], and M13mp18 cdsDNA
585 was prepared as previously described [62–64]. The M13mp18 nicked dsDNA (from here onward
586 called pEAW951) was prepared by nicking with DNaseI according to manufacturer's
587 recommendations. All DNA concentrations are given in terms of total nucleotides.

588 *ATPase Assay*

589 ATP hydrolysis of wild-type RecA and RecA(E38K) on nicked cdsDNA was measured
590 using a spectrophotometric enzyme assay [65,66]. ATP regeneration from phosphoenolpyruvate
591 and ADP was coupled to the oxidation of NADH, which was monitored by the decrease in
592 absorbance of NADH at 380 nm. 380-nm light was used so that the signal remained within the
593 linear range of the spectrophotometer during the experiment. The assays were carried out on a
594 Varian Cary 300 dual beam spectrophotometer equipped with a temperature controller and a 12-
595 position cell changer. The cell path length and band pass were 0.5 cm and 2 nm, respectively.
596 The NADH extinction coefficient at 380 nm of 1.21 mM^{-1} cm^{-1} was used to calculate the rate of
597 ATP hydrolysis.

598 The reactions were carried out at 37 ˚C in a buffer containing 25mM Tris-Ac (80%
599 cation, pH 7.5), 3 mM potassium glutamate, 10 mM magnesium acetate, 5% (w/v) glycerol,
600 1mM dithiothreitol, an ATP regeneration system (10 units/ml pyruvate kinase, 3.0 mM
601 phosphoenolpyruvate), and a coupling system (2 mM NADH and 10 units/ml lactate
602 dehydrogenase). The concentration of DNA (pEAW951 nicked cdsDNA) was 5μM. One cuvette
603 was a blank control that contained everything except the DNA (volume compensated with TE).
604 The nicked cdsDNA, buffer, and ATP regeneration system were preincubated at 37 ˚C for 10
605 min before addition of 3 mM ATP and 3 μM wild-type RecA or RecA(E38K). Data collection
606 was then begun.

607 *LexA Cleavage Assay*

608 The cleavage of LexA was performed essentially as previously described [27]. Reaction
609 mixtures (125μl) contained 40 mM Tris-HCl at pH 8.0, 10 mM $MgCl_2$, 30 mM NaCl, 2 mM
610 dithiothreitol, 3 μM of M13mp18 circular single-stranded DNA or pEAW951 nicked circular
611 double-stranded DNA, 3 mM ATPγS, LexA, and RecA as noted. Reactions were incubated at
612 37˚C for 10 minutes before addition of LexA. The reaction products were separated and
613 visualized by 15% SDS-PAGE stained with Coomassie blue.

614 *Analysis of colocalisation events of pol IV with replisomes*

615 Foci were classed as colocalised if their centroid positions (determined using our peak
616 fitter tool) fell within 2.18 pixels (218 nm) of each other [67]. For colocalisation analysis, we
617 binned the data in 30 min intervals for a larger sample size per time point due to low numbers of
618 pol IV foci per cell at exposures of 300 ms. We determined that for DinB-YPet–τ-mKate2
619 localisation the background of pol IV foci expected to colocalise with replisomes purely by

620 chance is ~4%. This was calculated by taking the area of each cell occupied by replisome foci
621 (including the colocalisation search radius) and dividing by the total area of the cell. The value of
622 4% corresponds to the mean of measurements made over > 300 cells. As the number of pol IV
623 foci changes in time, the proportion of replisome foci expected to colocalise with pol IV foci by
624 chance also changes in time. At an exposure time of 50 ms, there are almost zero pol IV foci at
625 the beginning of the measurement, thus there is close to zero probability that a replisome focus
626 will colocalise with a pol IV focus by chance. At t = 30 min, chance colocalisation is expected to
627 be 5% and at t = 120 min, the chance colocalisation is expected to be 3%. At an exposure time of
628 300 ms, the number of pol IV foci per cell never exceeds ~0.6 foci per cell, thus the level of
629 colocalisation expected to occur by chance is close to zero.

630 *Analysis of pol IV binding kinetics*

631 Replisome localisations were determined by identifying and fitting peaks from τ-mKate2
632 images. From the corresponding burst acquisition movie, the DinB-YPet signal at replisomes
633 was plotted against time (trajectories of DinB-YPet activity at replisomes) from 20–45 min, from
634 55–85 min and from 120–180 min after ciprofloxacin treatment (**S2C Fig**). These were divided
635 into trajectories that give and not give pol IV binding events (**S2D, E Fig**). From this, the
636 percentage of replisomes (τ-mKate2 foci) that are visited by DinB-YPet molecules (**Fig 4G**, right
637 panel) is calculated.

638 Only trajectories that have pol IV binding events were then used to separate pol IV
639 binding kinetics. The autocorrelation function was applied to each of these trajectories giving
640 signal similarities as a function of the lag time, a method that identifies time-dependent
641 fluctuations in signal dependent on binding and dissociation of molecules. When applying the
642 autocorrelation function to a DinB-YPet trajectory, the correlation of this trajectory with its time

643 delayed copy is generated for various lag times. With zero lag time, the normalised correlation of
644 a trajectory with itself is 1. The correlation of a trajectory with its time delayed copy, however,
645 gives autocorrelation values that range from 0–1 depending on signal fluctuations. DinB-YPet
646 molecules that are statically bound show no fluctuations in the DinB-YPet fluorescence signal
647 over time, consistent with the signal being correlated in time. Consequently, the autocorrelation
648 is between 0–1 for lag times after zero. In contrast, DinB-YPet molecules that are transiently
649 associated show many fluctuations in the DinB-YPet fluorescence signal over time. The signal is
650 not correlated in time and results in zero autocorrelation for lag times after zero.

651 For each time window (20–45 min, 55–85 min and 120–180 min), the mean
652 autocorrelation function output was calculated to determine the average of DinB-YPet binding
653 kinetics. The fast decay at t = 0 s corresponds to fast components. From t > 0 s, the curve was
654 fitted with a two-exponential function where medium or slow components were identified
655 ($y=y_0+A_1 \cdot e^{-x \cdot \tau 1}+A_2 \cdot e^{-x \cdot \tau 2}$). Using the *in vitro* experimentally determined rate of nucleotide
656 incorporation of pol IV as a guide (3–5 nt s^{-1} [52]), the fast, medium and slow components are
657 translated to no binding/short-lived binding (unproductive binding), binding events that are
658 sufficient for the insertion of 1–2 nucleotides or ~10 nucleotides, respectively.

659 Pol IV binding activity away from replisomes was determined as described above. Pol IV
660 trajectories were, however sampled, from average projections of pol IV burst acquisitions in time
661 (average projection over 100 frames, exposure time for each frame was 34 ms; total exposure 3.4
662 s; see **Fig 2**, upper row).

663 *Analysis of colocalisation events of pol IV with mCI*

664 To measure colocalisation between pol IV and mCI, we first created a maximum
665 projection of each PAmCherry-mCI movie. Similar to the colocalisation analysis performed for

666 pol IV with replisomes, foci were classed as colocalised if their centroid positions fell within 218
667 nm of each other. Chance colocalisation of pol IV with mCI is close to zero at 0 min. Chance
668 colocalisation is increased from 50 min with ~4%. At 100 min, the chance colocalisation is
669 ~15%.

670 **Acknowledgements**

671 We thank John P. McDonald for the pJM1243 plasmid and Roger Woodgate for RW880,
672 RW1594 and RW1598 strains, and pRW66 plasmid. We also thank Richard Spinks for helpful
673 discussions. MMC was supported by grant GM32335 from the National Institute of General
674 Medical Sciences USA. AvO was supported by a Laureate Fellowship FL140100027 from the
675 Australian Research Council. MFG was supported by grant R35ES028343 from the National
676 Institute of Environmental Health Sciences USA. AR was supported by Project Grant
677 APP1165135 from the National Health and Medical Research Council and funds from the
678 Faculty of Science, Medicine and Health and the Illawarra Health and Medical Research
679 Institute.

680 **Conflict of interest**

681 The authors declare no conflict of interest.

682 **References and Notes**

683 1. Napolitano R, Janel-Bintz R, Wagner J, Fuchs RPP. All three SOS-inducible DNA
684 polymerases (Pol II, Pol IV and Pol V) are involved in induced mutagenesis. EMBO J.
685 2000;19: 6259–6265.

686 2. Kumari A, Minko IG, Harbut MB, Finkel SE, Goodman MF, Lloyd RS. Replication
687 bypass of interstrand cross-link intermediates by *Escherichia coli* DNA polymerase IV. J
688 Biol Chem. 2008;283: 27433–27437.

689 3. Ikeda M, Furukohri A, Philippin G, Loechler E, Akiyama MT, Katayama T, et al. DNA
690 polymerase IV mediates efficient and quick recovery of replication forks stalled at N^2-dG
691 adducts. Nucleic Acids Res. 2014;42: 8461–8472.

692 4. Yuan B, Cao H, Jiang Y, Hong H, Wang Y. Efficient and accurate bypass of N^2-(1-
693 carboxyethyl)-2'-deoxyguanosine by DinB DNA polymerase *in vitro* and *in vivo.* Proc
694 Natl Acad Sci USA. 2008;105: 8679–9684.

695 5. Cafarelli TM, Rands TJ, Godoy VG. The DinB RecA complex of *Escherichia coli*
696 mediates an efficient and high-fidelity response to ubiquitous alkylation lesions. Environ
697 Mol Mutagen Mutagen. 2014;55: 92–102.

698 6. Jarosz DF, Godoy VG, Delaney JC, Essigmann JM, Walker GC. A single amino acid
699 governs enhanced activity of DinB DNA polymerases on damaged templates. Nature.
700 2006;439: 225–228.

701 7. Kim SR, Maenhaut-Michel G, Yamada M, Yamamoto Y, Matsui K, Sofuni T, et al.
702 Multiple pathways for SOS-induced mutagenesis in *Escherichia coli*: an overexpression of

703 *dinB/dinP* results in strongly enhancing mutagenesis in the absence of any exogenous
704 treatment to damage DNA. Proc Natl Acad Sci USA. 1997;94: 13792–13797.

705 8. Fuchs RP. Tolerance of lesions in *E. coli*: Chronological competition between translesion
706 synthesis and damage avoidance. DNA Repair. 2016;44: 51–58.

707 9. Henrikus SS, van Oijen AM, Robinson A. Specialised DNA polymerases in *Escherichia*
708 *coli*: roles within multiple pathways. Curr Genet. 2018;0: 1–8.

709 10. Fuchs RP, Fujii S. Translesion DNA synthesis and mutagenesis in prokaryotes. Cold
710 Spring Harb Perspect Biol. 2013;5: a012682.

711 11. Kath JE, Jergic S, Heltzel JMH, Jacob DT, Dixon NE, Sutton MD, et al. Polymerase
712 exchange on single DNA molecules reveals processivity clamp control of translesion
713 synthesis. Proc Natl Acad Sci USA. 2014;111: 7647–7652.

714 12. Henrikus SS, Wood EA, McDonald JP, Cox MM, Woodgate R, Goodman MF, et al. DNA
715 polymerase IV primarily operates outside of DNA replication forks in *Escherichia coli.*
716 PLoS Genet. 2018;14: e1007161.

717 13. Lovett ST. Replication arrest-stimulated recombination: Dependence on the RecA
718 paralog, RadA/Sms and translesion polymerase, DinB. DNA Repair. 2006;5: 1421–1427.

719 14. Pomerantz RT, Goodman MF, O'Donnell ME. DNA polymerases are error-prone at
720 RecA-mediated recombination intermediates. Cell Cycle. 2013;12: 2558–2563.

721 15. Shee C, Ponder R, Gibson JL, Rosenberg SM. What limits the efficiency of double-strand
722 break-dependent stress-induced mutation in *Escherichia coli*? J Mol Microbiol
723 Biotechnol. 2012;21: 8–19.

724 16. Williams AB, Hetrick KM, Foster PL. Interplay of DNA repair, homologous
725 recombination, and DNA polymerases in resistance to the DNA damaging agent 4-
726 nitroquinoline-1-oxide in *Escherichia coli*. DNA Repair. 2010;9: 1090–1097.

727 17. Pomerantz RT, Kurth I, Goodman MF, O'Donnell M. Preferential D-loop extension by a
728 translesion DNA polymerase underlies error-prone recombination. Nat Struct Mol Biol.
729 2013;20: 748–755.

730 18. Shee C, Gibson JL, Rosenberg SM. Two mechanisms produce mutation hotspots at DNA
731 breaks in *Escherichia coli*. Cell Rep. 2012;2: 714–721.

732 19. Shee C, Gibson JL, Darrow MC, Gonzalez C, Rosenberg SM. Impact of a stress-inducible
733 switch to mutagenic repair of DNA breaks on mutation in *Escherichia coli*. Proc Natl
734 Acad Sci USA. 2011;108: 13659–13664.

735 20. Cohen SE, Godoy VG, Walker GC. Transcriptional Modulator NusA Interacts with
736 translesion DNA polymerases in *Escherichia coli*. J Bacteriol. 2009;191: 665–672.

737 21. Kang P, Liao M, Wester MR, Leeder JS, Pearce RE. The transcription elongation factor
738 NusA is required for stress-induced mutagenesis in *Escherichia coli*. Curr Biol. 2010;20:
739 80–85.

740 22. Cohen SE, Lewis CA, Mooney RA, Kohanski MA, Collins JJ, Landick R, et al. Roles for
741 the transcription elongation factor NusA in both DNA repair and damage tolerance
742 pathways in *Escherichia coli*. Proc Natl Acad Sci USA. 2010;107: 15517–15522.

743 23. Cohen SE, Walker GC. New discoveries linking transcription to DNA repair and damage
744 tolerance pathways. Transcription. 2011;2: 37–40.

745 24. Godoy VG, Jarosz DF, Simon SM, Abyzov A, Walker GC. UmuD and RecA directly
746 modulate the mutagenic potential of the Y-family DNA polymerase DinB. Mol Cell.
747 2007;28: 1058–1070.

748 25. Frank EG, Ennis DG, Gonzalez M, Levine a S, Woodgate R. Regulation of SOS
749 mutagenesis by proteolysis. Proc Natl Acad Sci USA. 1996;93: 10291–6.

750 26. Woodgate R, Ennis DG. Levels of chromosomally encoded Umu proteins and
751 requirements for *in vivo* UmuD cleavage. Mol Genet Genomics. 1991;229: 10–16.

752 27. Burckhardt SE, Woodgate R, Scheuermann RH, Echols H, Battista JR, Ohta T, et al.
753 UmuD mutagenesis protein of *Escherichia coli*: overproduction, purification, and
754 cleavage by RecA. Proc Natl Acad Sci USA. 1988;85: 1811–1815.

755 28. Jiang Q, Karata K, Woodgate R, Cox MM, Goodman MF. The active form of DNA
756 polymerase V is UmuD′2C–RecA–ATP. Nature. 2009;460: 359–363.

757 29. Moore JM, Correa R, Rosenberg SM, Hastings PJ. Persistent damaged bases in DNA
758 allow mutagenic break repair in *Escherichia coli*. PLoS Genet. 2017;13: e1006733.

759 30. Ponder RG, Fonville NC, Rosenberg SM. A switch from high-fidelity to error-prone DNA
760 double-strand break repair underlies stress-induced mutation. Mol Cell. 2005;19: 791–
761 804.

762 31. Foster PL. Stress-induced mutagenesis in bacteria. Crit Rev Biochem Mol Biol. 2007;42:
763 373–397.

764 32. Rosenberg SM, Shee C, Frisch RL, Hastings PJ. Stress-induced mutation via DNA breaks
765 in *Escherichia coli*: A molecular mechanism with implications for evolution and

766 medicine. Bioessays. 2012;34: 885–892.

767 33. Mallik S, Popodi EM, Hanson AJ, Foster PL. Interactions and localization of *Escherichia*
768 *coli* error-prone DNA polymerase IV after DNA damage. J Bacteriol. 2015;197: 2792–
769 2809.

770 34. Henrikus SS, Henry C, Mcdonald JP, Hellmich Y, Wood EA, Woodgate R, et al. DNA
771 double-strand breaks induced by reactive oxygen species promote DNA polymerase IV
772 activity in *Escherichia coli*. bioRχiv. 2019; doi:http://dx.doi.org/10.1101/533422.

773 35. Cox MM. Regulation of bacterial RecA protein function. Crit Rev Biochem Mol Biol.
774 2007;42: 41–63. doi:10.1080/10409230701260258

775 36. Indiani C, Patel M, Goodman MF, O'Donnell ME. RecA acts as a switch to regulate
776 polymerase occupancy in a moving replication fork. Proc Natl Acad Sci USA. 2013;110:
777 5410–5415.

778 37. Tashjian TF, Danilowicz C, Molza A-E, Nguyen BH, Prévost C, Prentiss M, et al.
779 Residues in the fingers domain of the translesion DNA polymerase DinB enable its unique
780 participation in error-prone double strand break repair. J Biol Chem. 2019;
781 jbc.RA118.006233.

782 38. Ghodke H, Paudel B, Lewis JS, Jergic S, Gopal K, Romero Z, et al. Spatial and temporal
783 organization of RecA in the Escherichia coli DNA-damage response. Elife. 2019;8:
784 e42761. doi:https://doi.org/10.1101/413880

785 39. Renzette N, Gumlaw N, Nordman JT, Krieger M, Yeh S-P, Long E, et al. Localization of
786 RecA in *Escherichia coli* K-12 using RecA-GFP. Mol Microbiol. 2005;57: 1074–1085.

787 40. Wang TC, Chang HY, Hung JL. Cosuppression of *recF*, *recR* and *recO* mutations by
788 mutant *recA* alleles in *Escherichia coli* cells. Mutagen Res. 1993;294: 157–166.

789 41. Cazaux C, Mazard AM, Defais M. Inducibility of the SOS response in a *recA730* or
790 *recA441* strain is restored by transformation with a new *recA* allele. Mol Genet Genomics.
791 1993;240: 296–301.

792 42. Ennis DG, Levine AS, Koch WH, Woodgate R. Analysis of *recA* mutants with altered
793 SOS functions. Mutat Res. 1995;336: 39–48.

794 43. Churchward G, Belin D, Nagamine Y. A pSC101-derived plasmid which shows no
795 sequence homology to other commonly used cloning vectors. Gene. 1984;31: 165–171.

796 44. Woodgate R, Rajagopalan M, Lu C, Echols H. UmuC mutagenesis protein of *Escherichia*
797 *coli*: Purification and interaction with UmuD and UmuD′. Proc Natl Acad Sci USA.
798 1989;86: 7301–7305.

799 45. Drlica K, Zhao X. DNA gyrase, topoisomerase IV, and the 4-quinolones. Microbiol Mol
800 Biol Rev. 1997;61: 377–392.

801 46. Zhao X, Xu C, Domagala J, Drlica K. DNA topoisomerase targets of the
802 fluoroquinolones: a strategy for avoiding bacterial resistance. Proc Natl Acad Sci USA.
803 1997;94: 13991–13996.

804 47. Goswami M, Mangoli SH, Jawali N. Involvement of reactive oxygen species in the action
805 of ciprofloxacin against *Escherichia coli*. Future Microbiol. 2014;6: 949–954.

806 48. Gruenig MC, Renzette N, Long E, Chitteni-Pattu S, Inman RB, Cox MM, et al. RecA-
807 mediated SOS induction requires an extended filament conformation but no ATP

808 hydrolysis. Mol Microbiol. 2008;69: 1165–1179.

809 49. Simmons LA, Foti JJ, Cohen SE, Walker GC. The SOS regulatory network. EcoSal Plus.
810 2008;3: doi:10.1128/ecosalplus.5.4.3.

811 50. Silva MC, Nevin P, Ronayne EA, Beuning PJ. Selective disruption of the DNA
812 polymerase III α-β complex by the *umuD* gene products. Nucleic Acids Res. 2012;40:
813 5511–5522.

814 51. Sutton MD, Opperman T, Walker GC. The Escherichia coli SOS mutagenesis proteins
815 UmuD and UmuD′ interact physically with the replicative DNA polymerase. Proc Natl
816 Acad Sci USA. 1999;96: 12373–12378.

817 52. Wagner J, Fujii S, Gruz P, Nohmi T, Fuchs RPP. The beta clamp targets DNA polymerase
818 IV to DNA and strongly increases its processivity. EMBO Rep. 2000;1: 484–488.

819 53. Jaszczur MM, Bertram JG, Robinson A, van Oijen AM, Woodgate R, Cox MM, et al.
820 Mutations for worse or better: Low fidelity DNA synthesis by SOS DNA polymerase V is
821 a tightly-regulated double-edged sword. Biochemistry. 2016;2: 2309–2318.

822 54. Naiman K, Pagès V, Fuchs RP. A defect in homologous recombination leads to increased
823 translesion synthesis in *E. coli*. Nucleic Acids Res. 2016;44: 7691–7699.

824 55. Heltzel JMH, Maul RW, Wolff DW, Sutton MD. *Escherichia coli* DNA polymerase IV
825 (Pol IV), but not Pol II, dynamically switches with a stalled Pol III* replicase. J Bacteriol.
826 2012;194: 3589–3600.

827 56. Blattner FR, Plunkett III G, Bloch CA, Perna NT, Burland V, Riley M, et al. The complete
828 genome sequence of *Escherichia coli* K-12. Science. 1997;277: 1453–1474.

829 57. McDonald JP, Frank EG, Levine AS, Woodgate R. Intermolecular cleavage by UmuD-
830 like mutagenesis proteins. Proc Natl Acad Sci USA. 1998;95: 1478–1483.

831 58. Robinson A, McDonald JP, Caldas VEA, Patel M, Wood EA, Punter CM, et al.
832 Regulation of mutagenic DNA polymerase V activation in space and time. PLoS Genet.
833 2015;11: e1005482.

834 59. Schneider CA, Rasband WS, Eliceiri KW. NIH Image to ImageJ: 25 years of image
835 analysis. Nat Methods. 2012;9: 671–675.

836 60. Craig NL, Roberts JW. Function of nucleoside triphosphate and polynucleotide in
837 *Escherichia coli recA* protein-directed cleavage of phage λ repressor. J Biol Chem.
838 1981;256: 8039–8044.

839 61. Cox MM, Lusetti SL, Korth J, Modica MJ, Roca AI, Inman RB, et al. C-terminal
840 deletions of the *Escherichia coli* RecA protein . J Biol Chem. 2003;278: 16372–16380.

841 62. Neuendorf SK, Cox MM. Exchange of RecA protein between adjacent RecA protein-
842 single-stranded DNA complexes. J Biol Chem. 1986;261: 8276–8282.

843 63. Messing J. New M13 vectors for cloning. Methods Enzymol. 1983;101: 20–78.

844 64. Haruta N, Yu X, Yang S, Egelman EH, Cox MM. A DNA Pairing-enhanced conformation
845 of bacterial RecA proteins. J Biol Chem. 2003;278: 52710–52723.

846 65. Lindsleys E, Cox MM. Assembly and disassembly of RecA protein filaments opposite
847 filament ends occur at opposite filament ends. J Biol Chem. 1990;265: 9043–9054.

848 66. Morrical SW, Cox MM. Stabilization of RecA protein-ssDNA complexes by the single-

849 stranded DNA binding protein of *Escherichia coli*. Biochemistry. 1990;29: 837–843.

850 67. Henrikus SS, Henry C, Ghodke H, Wood EA, Mbele N, Saxena R, et al. RecFOR epistasis
851 group: RecF and RecO have distinct localizations and functions in *Escherichia coli*.
852 Nucleic Acids Res. 2019;47: 2946–2965.

853

855 **Table and figure legends**

856 **Table 1.** Strains used in this study.

857 **Figure 1. Number of DinB foci per cell and colocalisation measurements between DinB and**
858 **τ in different *umuDC* mutants following ciprofloxacin treatment.** (A) Upper panel: Number
859 of DinB foci per cell in *umuDC*$^+$ at 300 ms exposures. Error bar represents standard error of the
860 mean for n > 100 cells. Middle panel: Colocalisation percentage of DinB with DnaX (green
861 bars) in *umuDC*$^+$. Time points are binned over 30 min. Error bar represents standard error of the
862 mean between biological triplicates. Lower panel: Colocalisation percentage of DnaX with DinB
863 (magenta bars) in *umuDC*$^+$. Time points are binned over 30 min. The other columns represent the
864 same measurements as in (A), except from the cell strains (B) Δ*umuDC*, (C) Δ*umuDC* +
865 UmuD(K97A) expressed from a plasmid, and (D) Δ*umuDC* + UmuD′ expressed from a plasmid.

866 **Figure 2. Binding activity of DinB at and away from replisomes in different *umuDC***
867 **mutants.** (A) **Upper panel**: Images of DinB and DnaX signal in *umuDC*$^+$. Left: Projection of
868 DinB signal consistent with 300 ms exposure times. Right: Merged images of discoidal filtered
869 DinB (green) and DnaX signal (magenta). **Second panel from the top**: Exemplary trajectory
870 showing DinB activity at replisomes in *umuDC*$^+$. **Third panel from the top**: Mean
871 autocorrelation function showing DinB activity at replisomes in *umuDC*$^+$ at 25–45 (light grey
872 line), 55–85 (grey line) and 120–150 min (black line). Error bars represent standard error of the
873 mean over > 100 trajectories. **Bottom panel**: Components of the autocorrelation function for
874 DinB at replisomes in *umuDC*$^+$ showing fast (< 0.03 s, grey), medium (0.3 s, light green) and
875 slow components (1.7 s, dark green). The error bars for slow and medium components were
876 extracted from the fit error using the two-exponential fit (**Suppl. Fig 1G, H**). The error bar from

877 the fast components is equivalent to the standard error of the mean from the mean
878 autocorrelation function at lag time 0s. (B) similar to (A), however in Δ*umuDC*. (C) similar to
879 (A), however in Δ*umuDC* + UmuD(K97A) expressed from a plasmid. (D) similar to (A),
880 however in Δ*umuDC* + UmuD′ expressed from a plasmid.

881 **Figure 3. Colocalisation measurement between DinB and mCI after ciprofloxacin**
882 **treatment.** (A) Merged images of discoidal filtered DinB-YPet (green) and PAmCherry-mCI
883 (magenta) at 55, 70, 100 and 155 min after ciprofloxacin addition. (B) Colocalisation percentage
884 of DinB with mCI. Time points are binned over 30 min. Error bar represents standard deviation
885 of biological quadruplicates.

886 **Figure 4. Binding activity of DinB at and away from replisomes in different *lexA* and *recA***
887 **mutants.** (A) Images of DinB and DnaX signal in *lexA*$^+$ *recA*$^+$. Left: Projection of DinB signal
888 consistent with 300 ms exposure times. Right: Merged images of discoidal filtered DinB (green)
889 and DnaX signal (magenta). (B) similar to (A), however in *lexA*(Def) *recA*$^+$. (C) similar to (A),
890 however in *lexA*(Def) *recA*(E38K). (D) Left: DinB signal at a replisome in *lexA*$^+$ *recA*$^+$. Right:
891 DinB signal away from replisome in *lexA*$^+$ *recA*$^+$. (E) Left: DinB signal at a replisome in
892 *lexA*(Def) *recA*$^+$. Right: DinB signal away from replisome in *lexA*(Def) *recA*$^+$. (F) Left: DinB
893 signal at a replisome in *lexA*(Def) *recA*(E38K). Right: DinB signal away from replisome in
894 *lexA*(Def) *recA*(E38K). (G) Mean autocorrelation function showing DinB activity at replisomes
895 in *lexA*$^+$ *recA*$^+$ (black line), *lexA*(Def) *recA*$^+$ (grey line) and *lexA*(Def) *recA*(E38K) (green line).
896 Error bars represent standard error of the mean over > 100 trajectories. (H) Mean autocorrelation
897 function showing DinB activity away from replisomes in *lexA*$^+$ *recA*$^+$ (black line), *lexA*(Def)
898 *recA*$^+$ (grey line) and *lexA*(Def) *recA*(E38K) (green line). Error bars represent standard error of
899 the mean > 100 trajectories.

900 **Supplementary Figure S1. Colocalisation analysis using 50 ms exposures for DinB-YPet**
901 **and number of DinB-YPet and τ-mKate2 foci per cell.** (A) Upper row: colocalisation of DinB
902 with DnaX. Left plot compares *umuDC*$^+$ (black line) with Δ*umuDC* (green line). Middle plot
903 compares *umuDC*$^+$ (black line) with Δ*umuDC* + UmuD(K97A) expressed from plasmid (green
904 line). Right plot compares *umuDC*$^+$ (black line) with Δ*umuDC* + UmuD′ expressed from plasmid
905 (green line). Bottom row: colocalisation of DnaX with DinB. Left plot compares *umuDC*$^+$ (black
906 line) with Δ*umuDC* (green line). Middle plot compares *umuDC*$^+$ (black line) with Δ*umuDC* +
907 UmuD(K97A) expressed from plasmid (green line). Right plot compares *umuDC*$^+$ (black line)
908 with Δ*umuDC* + UmuD′ expressed from plasmid (green line). Error bars represent standard error
909 of the mean between at least biological triplicates. (B) Number of DinB (upper plot) and DnaX
910 foci per cell (bottom plot) in *umuDC*$^+$ (black line), Δ*umuDC* (red line), Δ*umuDC* +
911 UmuD(K97A) (yellow line) and Δ*umuDC* + UmuD′ (blue line) after ciprofloxacin treatment.
912 Error bars represent standard error of the mean for $n > 100$ cells.

913

914 **Supplementary Figure S2. Burst acquisitions and analysis.** (A) Experimental setup. Cells are
915 loaded in a flow cell and immobilised on a positively charged APTES glass surface. Cells were
916 imaged before addition of ciprofloxacin and 25–45, 55–85 and 120–150 min after addition. (B)
917 Burst acquisition sequence. Movies of DinB-YPet were recorded. The movies contain 300
918 frames at an exposure of 50 ms taken every 100 ms. Subsequently, an image of the τ-mKate2
919 channel is taken at an exposure time of 100 ms. (C) Exemplary intensity trajectories showing
920 DinB-YPet binding at replisomes. (D) Histogram of DinB-YPet intensities at replisomes. From
921 cut-off to 0: replisomes with no DinB-YPet binding. From cut-off to higher intensities:
922 replisomes with DinB-YPet binding. (E) Grouping of trajectories. Trajectories that show no

923 DinB-YPet binding at replisomes are excluded from the analysis. Trajectories that show DinB-
924 YPet binding at replisomes are used for the analysis. (F), The mean autocorrelation function is
925 obtained from single autocorrelation function. Each autocorrelation function stems from single
926 intensity trajectories of a DinB-YPet binding event at replisomes. (G), Determining components
927 of autocorrelation functions. The mean autocorrelation function is plotted in black. The
928 autocorrelation function has fast components which consist of noise, short-lived and transient
929 binding events (light grey line). Slower components are fitted with a two-exponential fit (green
930 line) which consist of medium and slow decorrelation events consistent with binding events. (H),
931 Components of the autocorrelation function are plotted in a bar graph. Slow, medium and fast
932 components are indicated by different colours: slow (dark green), medium (light green), fast
933 (light grey). The error bars for slow and medium components were extracted from the fit error
934 using the two-exponential fit. The error bar from the fast components is equivalent to the
935 standard error of the mean from the mean autocorrelation function at lag time 0s.

936 **Supplementary Figure S3. Sensorgram showing RecA(E38K) filament assembly on ssDNA**
937 **and dsDNA in order to probe interactions with pol IV.** (A) Sensorgram showing the
938 immobilisation of ssDNA, $(dT)_{71}$, on the SA chip surface (association: dark grey phase;
939 immobilised ssDNA: light grey phase). (B) Following ssDNA immobilisation, buffer containing
940 1 μM RecA(E38K) (+ 1 mM ATPγS) was flowed into the flow cell, at t = 0 min for 400 s.
941 During this period, RecA(E38K) associated with ssDNA (blue phase), forming a RecA(E38K)
942 filament. At 400 s, buffer containing 1 mM ATPγS was flowed into the flow cell. RecA(E38K)
943 dissociates from the surface (yellow phase). From 1,400 s, RU units are constant, consistent with
944 stabilised RecA(E38K) filaments. (C) Sensorgram showing the immobilisation of dsDNA on the
945 SA chip surface (association: dark grey phase; immobilised dsDNA: light grey phase). (D)

946 Following dsDNA immobilisation, buffer containing 1 μM RecA(E38K) (+ 0.5 mM ATPγS) was
947 flowed into the flow cell, at t = 0 min for 500 s. During this period, RecA(E38K) associated with
948 ssDNA (blue phase), forming a RecA(E38K) filament. From 500 – 3,000 s, buffer containing 0.5
949 or 1 mM ATPγS was flowed into the flow cell (yellow phase). From 3,000 – 7,200 s, buffer
950 containing 1 μM RecA(E38K) (+ 0.5 mM ATPγS) was flowed into the flow cell to allow for
951 more RecA(E38K) to associate with the dsDNA. (E) Sensorgram showing the association of pol
952 IV with RecA(E38K) structures formed on dsDNA. At t = 0 s, 0.65 uM pol IV (+ 0.5 mM
953 ATPγS) was flowed into the flow cell for 220 s and association of pol IV was observed (green
954 phase). At t = 220 s, buffer containing 0.5 mM ATPγS was flowed into the flow cell (yellow
955 phase). (F) Sensorgram showing the association of pol IV with dsDNA. At t = 0 s, 0.65 uM pol
956 IV (+ 0.5 mM ATPγS) was flowed into the flow cell for 220 s and association of pol IV was
957 observed (green phase). At t = 220 s, buffer containing 0.5 mM ATPγS was flowed into the flow
958 cell (yellow phase). Lower response units are recorded than for the association of pol IV with
959 RecA(E38K) structures on dsDNA.

960 **Supplementary Figure S4. RecA(E38K) forms RecA*-like structures on circular dsDNA.**
961 (A) RecA(E38K) readily binds to dsDNA. In six separate reactions, either RecA(E38K) or wild-
962 type RecA was incubated at 37 ˚C with nicked circular dsDNA (cdsDNA), ATP, and an ATP
963 regeneration system. (B) LexA Cleavage Assays. Reaction mixtures contained 40 mM Tris-HCl
964 at pH 8.0, 10 mM $MgCl_2$, 30 mM NaCl, 2 mM dithiothreitol, 3 μM circular single-stranded DNA
965 (cssDNA) or nicked circular double-stranded DNA (cdsDNA), 3 mM ATPγS, LexA, and RecA
966 as noted. Reactions were incubated at 37˚C for 10 minutes before addition of UmuD or LexA.
967 The reaction products were separated and visualized by 15% SDS-PAGE stained with
968 Coomassie blue. Lane 1 contains a protein ladder while subsequent groups of three lanes contain

969 the same reaction mixture sampled at 0, 20, and 40 minutes. On cssDNA, RecA(E38K) and wild-
970 type RecA form RecA* structures. On cdsDNA however, RecA(E38K) forms RecA*-like
971 structures in contrast to wildtype RecA.

972 **Supplementary Notes**

973 Sequence of pJMuvrA-PAmCherry-mCI vector:

974 AAGCTGGAAGATCTTCCCTGGCACGACAGGTTTCCCGACTGGAAAGCGGGCAGTGA
975 GCGCAACGCAATTAATGTGAGTTAGCTCACTCATTAGGCACCCCAGGCTTTACACTT
976 TATGCTTCCGGCTCGTATGTTGTGTGGAATTGTGAGCGGATAACAATTTCACACAGG
977 AAACAGCTATGACCATGATTACGCCAAGCGCGCAATTAACCCTCACTAAAGGGAAC
978 AAAAGCTGGGTACCGGGCCCCCCCTCGAGGTCGACTTCCGGGAAACAAACCTGGCC
979 AGACATTGTTACACAACACTCCGGGTAATGCATTCCAATACTGTATATTCATTCAGG
980 TCAATTTGTGTCATAATTAACCGTTTGTGATCGGATCCAGCACCATGCCACCGGGCA
981 AAAAAGCGTTTAATCCGGGAAAGCATATGGTGAGCAAGGGCGAGGAGGATAACAT
982 GGCCATCATTAAGGAGTTCATGCGCTTCAAGGTGCACATGGAGGGGTCCGTGAACG
983 GCCACGTGTTCGAGATCGAGGGCGAGGGCGAGGGCCGCCCCTACGAGGGCACCCAG
984 ACCGCCAAGCTGAAGGTGACCAAGGGTGGCCCCCTGCCCTTCACCTGGGACATCCT
985 GTCCCCTCAATTCATGTACGGCTCCAATGCCTACGTGAAGCACCCCGCCGACATCCC
986 CGACTACTTTAAGCTGTCCTTCCCCGAGGGCTTCAAGTGGGAGCGCGTGATGAAATT
987 CGAGGACGGCGGCGTGGTGACCGTGACCCAGGACTCCTCCCTGCAAGACGGTGAGT
988 TCATCTACAAGGTGAAGCTGCGCGGCACCAACTTCCCCTCCGACGGCCCCGTAATGC
989 AGAAGAAGACCATGGGCTGGGAGGCCCTCTCCGAGCGGATGTACCCCGAGGACGGC
990 GCCCTGAAGGGCGAGGTCAAGCCGCGCGTGAAGCTGAAGGACGGCGGCCACTACG

991 ACGCTGAGGTCAAGACCACCTACAAGGCCAAGAAGCCCGTGCAGCTGCCCGGCGCC

992 TACAACGTCAACCGCAAGTTGGACATCACCTCACACAACGAGGACTACACCATCGT

993 GGAACAGTACGAACGTGCCGAGGGCCGCCACTCCACCGGCGGCATGGACGAGCTGT

994 ACAAGGAGCTCGCTGCAGGTGGCGGCGGCGGCTCCGGCAGCCATATGTATGAGTAC

995 CCTGTTTTTTCTCATGTTCAGGCAGGGATGTTCTCACCTGAGCTTCGCACCTTTACCA

996 AAGGTGATGCGGAGCGCTGGGTAAGCACAACCAAAAAAGCCAGTGATTCTGCATTC

997 TGGCTTGAGGTTGAAGGTAATTCCATGACCACACCAACAGGCTCCAAGACAAGCTTT

998 CCTGACGGAATGTTAATTCTCGTTGACCCTGAGCAGGCTGTTGAGCCAGGTGATTTC

999 TGCATTGCCCGCCTTGGGGGTGATGAGTTTACCTTCGCGAAACTGATCCGCGATAGC

1000 GGTCAGGTGTTTTTACAACCACTGAACCCACAGTACCCAATGATCCCATGCAATGAG

1001 AGTTGTTCCGTTGTGGGGAAAGTTATCGCTAGTCAGTGAGCGGCCGCGAATTCGAAG

1002 TTCCTATAGTTTCTAGAGAATAGGAACTTCGATCTTTAGAAAAACTCATCGAGCATC

1003 AAATGAAACTGCAATTTATTCATATCAGGATTATCAATACCATATTTTTGAAAAAGC

1004 CGTTTCTGTAATGAAGGAGAAAACTCACCGAGGCAGTTCCATAGGATGGCAAGATC

1005 CTGGTATCGGTCTGCGATTCCGACTCGTCCAACATCAATACAACCTATTAATTTCCCC

1006 TCGTCAAAAATAAGGTTATCAAGTGAGAAATCACCATGAGTGACGACTGAATCCGG

1007 TGAGAATGGCAAAAGCTTATGCATTTCTTTCCAGACTTGTTCAACAGGCCAGCCATT

1008 ACGCTCGTCATCAAAATCACTCGCATCAACCAAACCGTTATTCATTCGTGATTGCGC

1009 CTGAGCGAGACGAAATACACGATCGCTGTTAAAAGGACAATTACAAACAGGAATCG

1010 AATGCAACCGGCGCAGGAACACTGCCAGCGCATCAACAATATTTTCACCTGAATCA

1011 GGATATTCTTCTAATACCTGGAATGCTGTTTTCCCGGGGATCGCAGTGGTGAGTAAC

1012 CATGCATCATCAGGAGTACGGATAAAATGCTTGATGGTCGGAAGAGGCATAAATTC

1013 CGTCAGCCAGTTTAGTCTGACCATCTCATCTGTAACATCATTGGCAACGCTACCTTTG

1014 CCATGTTTCAGAAACAACTCTGGCGCATCGGGCTTCCCATACAATCGATAGATTGTC

1015 GCACCTGATTGCCCGACATTATCGCGAGCCCATTTATACCCATATAAATCAGCATCC

1016 ATGTTGGAATTTAATCGCGGGCGCGAGCAAGACGTTTCCCGTTGAATATGGCTCATA

1017 ACACCCCTTGTATTACTGTTTATGTAAGCAGACAGTTTTATTGTTCATGATGATATAT

1018 TTTTATCTTGTGCAATGTAACATCAGAGATTTTGAGACACAACGTGGCTTTCCCCGCC

1019 CGCCCGATCCCCGGGTACCGAGCTCGAATTTCGACCAATTCGAAGTTCCTATACTTT

1020 CTAGAGAATAGGAACTTCCCGCGGTGGAGCTCCAATTCGCCCTATAGTGAGTCGTAT

1021 TACGCGCGCTCACTGGCCGTCGTTTTACAACGTCGTGACTGGGAAAACCCTGGCGTT

1022 ACCCAACTTAATCGCCTTGCAGCACATCCCCCTTTCGCCAGCTGGCGTAATAGCGAA

1023 GAGGCCCGCACCGATCGCCCTTCCCAACAGTTGCGCAGCCTGAATGGCGAATGGGA

1024 CGCGCCCTGTAGCGGCGCATTAAGCGCGGCGGGTGTGGTGGTTACGCGCAGCGTGA

1025 CCGCTACACTTGCCAGCGCCCTAGCGCCCGCTCCTTTCGCTTTCTTCCCTTCCTTTCTC

1026 GCCACGTTCGCCGGAAGATCTTCCAATTCCCGACAGTAAGACGGGTAAGCCTGTTGA

1027 TGATACCGCTGCCTTACTGGGTGCATTAGCCAGTCTGAATGACCTGTCACGGGATAA

1028 TCCGAAGTGGTCAGACTGGAAAATCAGAGGGCAGGAACTGCTGAACAGCAAAAAGT

1029 CAGATAGCACCACATAGCAGACCCGCCATAAAACGCCCTGAGAAGCCCGTGACGGG

1030 CTTTTCTTGTATTATGGGTAGTTTCCTTGCATGAATCCATAAAAGGCGCCTGTAGTGC

1031 CATTTACCCCCATTCACTGCCAGAGCCGTGAGCGCAGCGAACTGAATGTCACGAAA

1032 AAGACAGCGACTCAGGTGCCTGATGGTCGGAGACAAAAGGAATATTCAGCGATTTG

1033 CCCGAGCTTGCGAGGGTGCTACTTAAGCCTTTAGGGTTTTAAGGTCTGTTTTGTAGA

1034 GGAGCAAACAGCGTTTGCGACATCCTTTTGTAATACTGCGGAACTGACTAAAGTAGT

1035 GAGTTATACACAGGGCTGGGATCTATTCTTTTTATCTTTTTTTATTCTTTCTTTATTCT

1036 ATAAATTATAACCACTTGAATATAAACAAAAAAAACACACAAAGGTCTAGCGGAAT

1037 TTACAGAGGGTCTAGCAGAATTTACAAGTTTTCCAGCAAAGGTCTAGCAGAATTTAC

1038 AGATACCCACAACTCAAAGGAAAAGGACTAGTAATTATCATTGACTAGCCCATCTC

1039 AATTGGTATAGTGATTAAAATCACCTAGACCAATTGAGATGTATGTCTGAATTAGTT

1040 GTTTTCAAAGCAAATGAACTAGCGATTAGTCGCTATGACTTAACGGAGCATGAAACC

1041 AAGCTAATTTTATGCTGTGTGGCACTACTCAACCCCACGATTGAAAACCCTACAAGG

1042 AAAGAACGGACGGTATCGTTCACTTATAACCAATACGCTCAGATGATGAACATCAG

1043 TAGGGAAAATGCTTATGGTGTATTAGCTAAAGCAACCAGAGAGCTGATGACGAGAA

1044 CTGTGGAAATCAGGAATCCTTTGGTTAAAGGCTTTGAGATTTTCCAGTGGACAAACT

1045 ATGCCAAGTTCTCAAGCGAAAAATTAGAATTAGTTTTTAGTGAAGAGATATTGCCTT

1046 ATCTTTTCCAGTTAAAAAAATTCATAAAATATAATCTGGAACATGTTAAGTCTTTTG

1047 AAAACAAATACTCTATGAGGATTTATGAGTGGTTATTAAAAGAACTAACACAAAAG

1048 AAAACTCACAAGGCAAATATAGAGATTAGCCTTGATGAATTTAAGTTCATGTTAATG

1049 CTTGAAAATAACTACCATGAGTTTAAAAGGCTTAACCAATGGGTTTTGAAACCAATA

1050 AGTAAAGATTTAAACACTTACAGCAATATGAAATTGGTGGTTGATAAGCGAGGCCG

1051 CCCGACTGATACGTTGATTTTCCAAGTTGAACTAGATAGACAAATGGATCTCGTAAC

1052 CGAACTTGAGAACAACCAGATAAAAATGAATGGTGACAAAATACCAACAACCATTA

1053 CATCAGATTCCTACCTACATAACGGACTAAGAAAAACACTACACGATGCTTTAACTG

1054 CAAAAATTCAGCTCACCAGTTTTGAGGCAAAATTTTTGAGTGACATGCAAAGTAAGT

1055 ATGATCTCAATGGTTCGTTCTCATGGCTCACGCAAAAACAACGAACCACACTAGAGA

1056 ACATACTGGCTAAATACGGAAGGATCTGAGGTTCTTATGGCTCTTGTATCTATCAGT

1057 GAAGCATCAAGACTAACAAACAAAAGTAGAACAACTGTTCACCGTTACATATCAAA

1058 GGGAAAACTGTCCATATATGCACAGATGAAAACGGTGTAAAAAAGATAGATACATC

1059 AGAGCTTTTACGAGTTTTTGGTGCATTCAAAGCTGTTCACCATGAACAGATCGACAA

1060 TGTAACAGATGAACAGCATGTAACACCTAATAGAACAGGTGAAACCAGTAAAACAA

1061 AGCAACTAGAACATGAAATTGAACACCTGAGACAACTTGTTACAGCTCAACAGTCA

1062 CACATAGACAGCCTGAAACAGGCGATGCTGCTTATCGAATCAAAGCTGCCGACAAC

1063 ACGGGAGCCAGTGACGCCTCCCGTGGGGAAAAAATCATGGCAATTCTGGAAGAAAT

1064 AGCGCTTTCAGCCGGCAAACCTGAAGCCGGATCTGCGATTCTGATAACAAACTAGC

1065 AACACCAGAACAGCCCGTTTGCGGGCAGCAAAACCCGTGGGAATTAATTCCCCTGC

1066 TCGCGCAGGCTGGGTGCCAAGCTCTCGGGTAACATCAAGGCCCGATCCTTGGAGCC

1067 CTTGCCCTCCCGCACGATGATCGTGCCGTGATCGAAATCCAGATCCTTGACCCGCAG

1068 TTGCAAACCCTCACTGATCCGCATGCCCGTTCCATACAGAAGCTGGGCGAACAAAC

1069 GATGCTCGCCTTCCAGAAAACCGAGGATGCGAACCACTTCATCCGGGGTCAGCACC

1070 ACCGGCAAGCGCCGCGACGGCCGAGGTCTTCCGATCTCCTGAAGCCAGGGCAGATC

1071 CGTGCACAGCACCTTGCCGTAGAAGAACAGCAAGGCCGCCAATGCCTGACGATGCG

1072 TGGAGACCGAAACCTTGCGCTCGTTCGCCAGCCAGGACAGAAATGCCTCGACTTCG

1073 CTGCTGCCCAAGGTTGCCGGGTGACGCACACCGTGGAAACGGATGAAGGCACGAAC

1074 CCAGTGGACATAAGCCTGTTCGGTTCGTAAGCTGTAATGCAAGTAGCGTATGCGCTC

1075 ACGCAACTGGTCCAGAACCTTGACCGAACGCAGCGGTGGTAACGGCGCAGTGGCGG

1076 TTTTCATGGCTTGTTATGACTGTTTTTTTGGGGTACAGTCTATGCCTCGGGCATCCAA

1077 GCAGCAAGCGCGTTACGCCGTGGGTCGATGTTTGATGTTATGGAGCAGCAACGATGT

1078 TACGCAGCAGGGCAGTCGCCCTAAAACAAAGTTAAACATCATGAGGGAAGCGGTGA

1079 TCGCCGAAGTATCGACTCAACTATCAGAGGTAGTTGGCGTCATCGAGCGCCATCTCG

1080 AACCGACGTTGCTGGCCGTACATTTGTACGGCTCCGCAGTGGATGGCGGCCTGAAGC

1081 CACACAGTGATATTGATTTGCTGGTTACGGTGACCGTAAGGCTTGATGAAACAACGC

1082 GGCGAGCTTTGATCAACGACCTTTTGGAAACTTCGGCTTCCCCTGGAGAGAGCGAGA

1083 TTCTCCGCGCTGTAGAAGTCACCATTGTTGTGCACGACGACATCATTCCGTGGCGTT

1084 ATCCAGCTAAGCGCGAACTGCAATTTGGAGAATGGCAGCGCAATGACATTCTTGCA

1085 GGTATCTTCGAGCCAGCCACGATCGACATTGATCTGGCTATCTTGCTGACAAAAGCA

1086 AGAGAACATAGCGTTGCCTTGGTAGGTCCAGCGGCGGAGGAACTCTTTGATCCGGTT

1087 CCTGAACAGGATCTATTTGAGGCGCTAAATGAAACCTTAACGCTATGGAACTCGCCG

1088 CCCGACTGGGCTGGCGATGAGCGAAATGTAGTGCTTACGTTGTCCCGCATTTGGTAC

1089 AGCGCAGTAACCGGCAAAATCGCGCCGAAGGATGTCGCTGCCGACTGGGCAATGGA

1090 GCGCCTGCCGGCCCAGTATCAGCCCGTCATACTTGAAGCTAGACAGGCTTATCTTGG

1091 ACAAGAAGAAGATCGCTTGGCCTCGCGCGCAGATCAGTTGGAAGAATTTGTCCACT

1092 ACGTGAAAGGCGAGATCACCAAGGTAGTCGGCAAATAATGTCTAACAATTCGTTCA

1093 AGCCGACGCCGCTTCGCGGCGCGGCTTAACTCAAGCGTTAGATGCACTAAGCACAT

1094 AATTGCTCACAGCCAAACTATCAGGTCAAGTCTGCTTTTATTATTTTTAAGCGTGCAT

1095 AATAAGCCCTACACAAATTGGGAGATATATCATGAAAGGCTGGCTTTTTCTTGTTAT

1096 CGCAATAGTTGGCGAAGTAATCGCAACATCCGCATTAAAATCTAGCGAGGGCTTTAC

1097 T

Figure 1

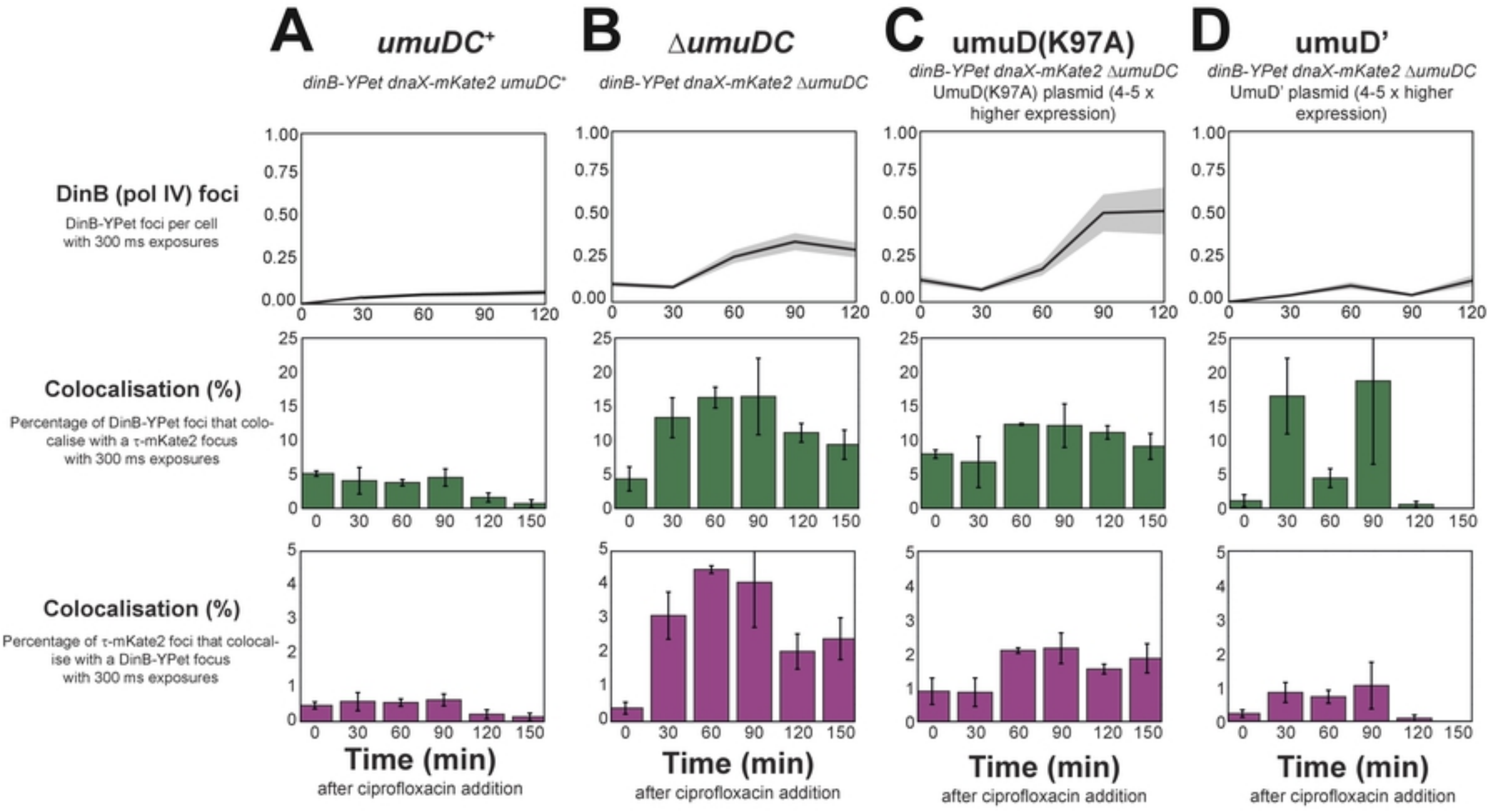
A
umuDC+
dinB-YPet dnaX-mKate2 umuDC+
B
ΔumuDC
dinB-YPet dnaX-mKate2 ΔumuDC
C
umuD(K97A)
dinB-YPet dnaX-mKate2 ΔumuDC
UmuD(K97A) plasmid (4-5 x higher expression)
D
umuD'
dinB-YPet dnaX-mKate2 ΔumuDC
UmuD' plasmid (4-5 x higher expression)
DinB (pol IV) foci
DinB-YPet foci per cell with 300 ms exposures
Colocalisation (%)
Percentage of DinB-YPet foci that colocalise with a τ-mKate2 focus with 300 ms exposures
Colocalisation (%)
Percentage of τ-mKate2 foci that colocalise with a DinB-YPet focus with 300 ms exposures
Time (min)
after ciprofloxacin addition

Figure 2

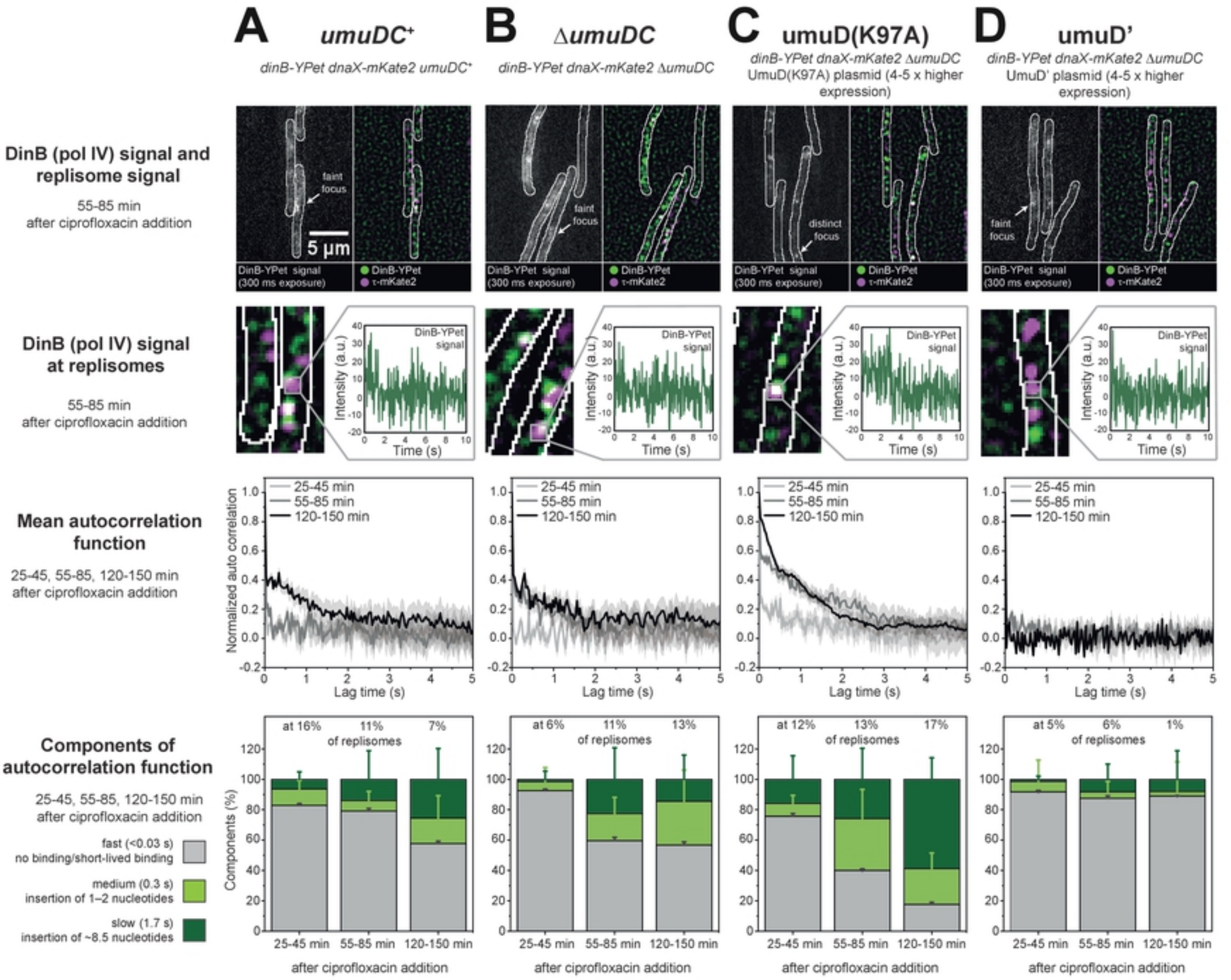
A umuDC+
B ΔumuDC
C umuD(K97A)
D umuD'
dinB-YPet dnaX-mKate2 umuDC+
dinB-YPet dnaX-mKate2 ΔumuDC
dinB-YPet dnaX-mKate2 ΔumuDC UmuD(K97A) plasmid (4-5 x higher expression)
dinB-YPet dnaX-mKate2 ΔumuDC UmuD' plasmid (4-5 x higher expression)
DinB (pol IV) signal and replisome signal
55-85 min after ciprofloxacin addition
faint focus
distinct focus
5 µm
DinB-YPet signal (300 ms exposure)
DinB-YPet
τ-mKate2
DinB (pol IV) signal at replisomes
55-85 min after ciprofloxacin addition
DinB-YPet signal
Intensity (a.u.)
Time (s)
Mean autocorrelation function
25-45, 55-85, 120-150 min after ciprofloxacin addition
25-45 min
55-85 min
120-150 min
Normalized auto correlation
Lag time (s)
Components of autocorrelation function
25-45, 55-85, 120-150 min after ciprofloxacin addition
fast (<0.03 s) no binding/short-lived binding
medium (0.3 s) insertion of 1–2 nucleotides
slow (1.7 s) insertion of ~8.5 nucleotides
at 16% 11% 7% of replisomes
at 6% 11% 13% of replisomes
at 12% 13% 17% of replisomes
at 5% 6% 1% of replisomes
Components (%)
after ciprofloxacin addition

Figure 3

A **Merged images:**
DinB-YPet and PAmCherry-mCI

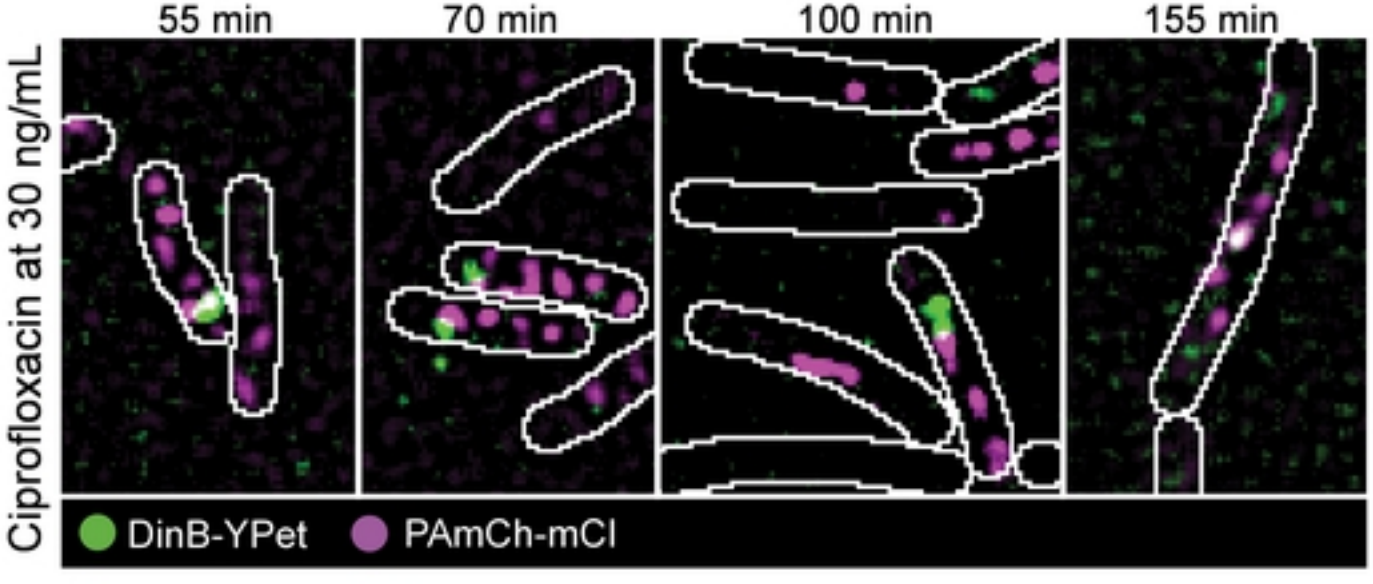

B **Colocalisation:**
DinB (pol IV) foci that contain an mCI focus

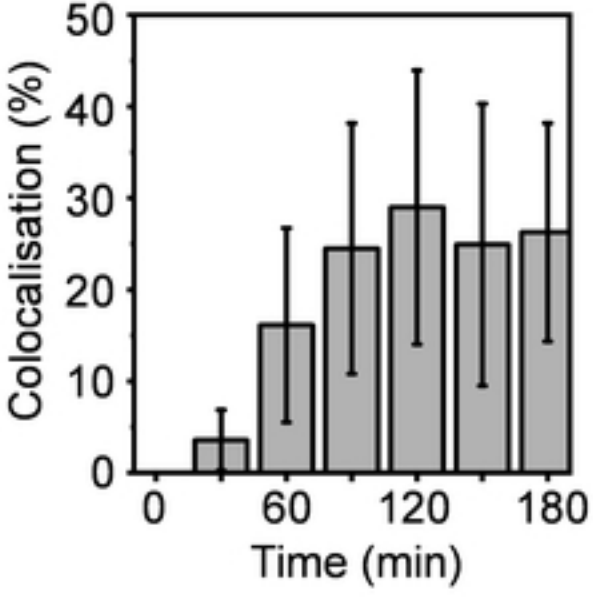

Figure 4

Images:

DinB (pol IV) signal and replisome signal

Examplary trajectories:

DinB (pol IV) signal at and away from replisomes

Mean autocorrelation function:
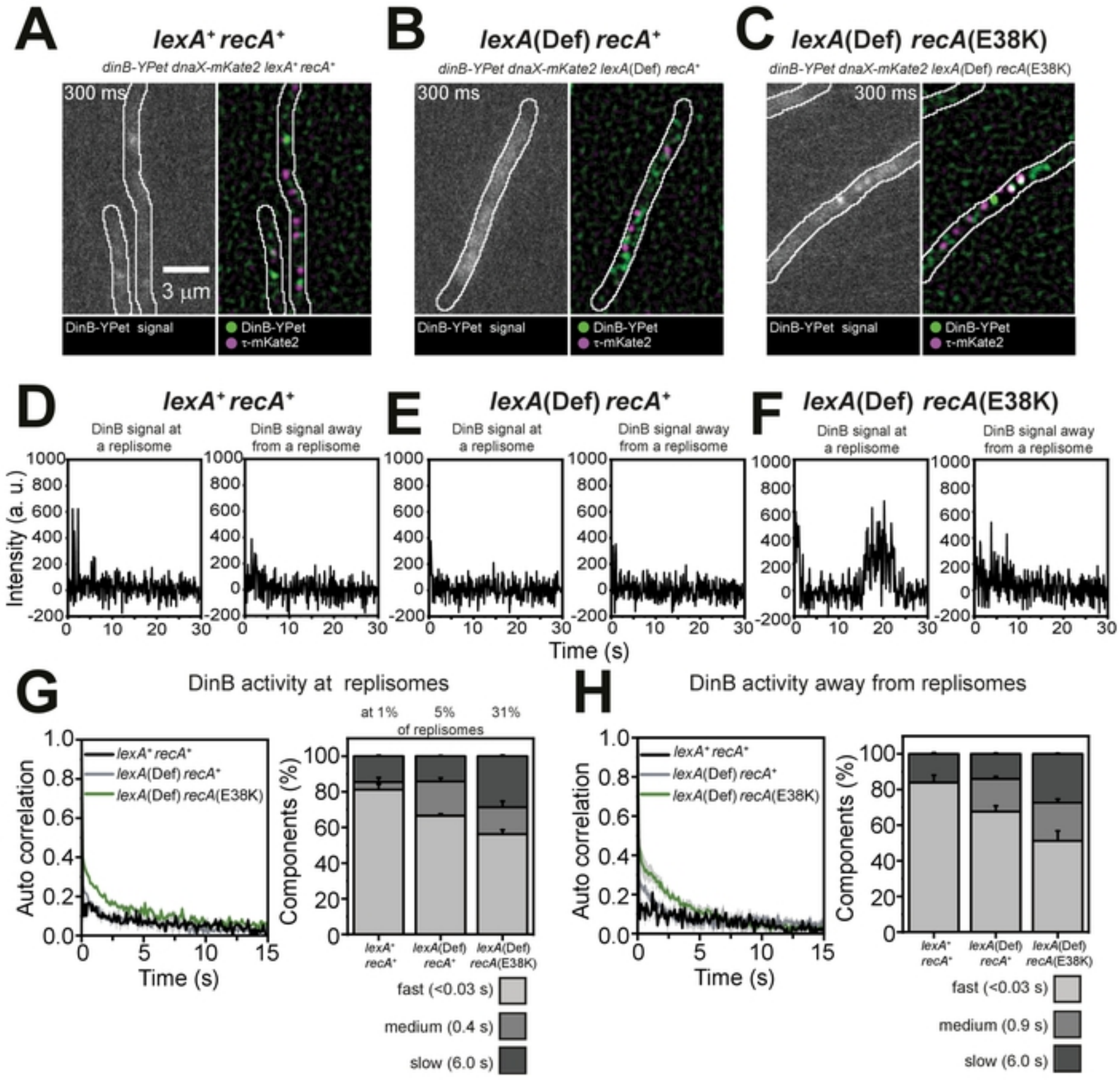
DinB (pol IV) signal at and away from replisomes